REPORT DOCUMENTATION PAGE

Form Approved
OMB No. 0704-0188

1. AGENCY USE ONLY (Leave blank)	2. REPORT DATE	3. REPORT TYPE AND DATES COVERED
	Sept. 15, 1990	Final, 15/6/87 - 15/6/90

4. TITLE AND SUBTITLE

Partitioning Reactions to Control and Develop Unique Microstructures

5. FUNDING NUMBERS

AFOSR-87-0291

6. AUTHOR(S)

F. F. Lange

AFOSR-TR- 90 1129

AD-A229 029

7. PERFORMING ORGANIZATION NAME(S) AND ADDRESS(ES)

Materials Department
College of Engineering
University of California
Santa Barbara, CA 93106

8. PERFORMING ORGANIZATION REPORT NUMBER

AFOSR Final and Technical Rept. No. 8

9. SPONSORING MONITORING AGENCY NAME(S) AND ADDRESS(ES)

AFOSR/NE
Building 410
Bolling AFB, D.C. 20332-6448

10. SPONSORING MONITORING AGENCY REPORT NUMBER

2306/A2

11. SUPPLEMENTARY NOTES

With Technical Rept. No. 8

12a. DISTRIBUTION AVAILABILITY STATEMENT

Unlimited

12b. DISTRIBUTION CODE

13. ABSTRACT (Maximum 200 words)

Studies reported include: 1) Liquid precursor formulation, pyrolysis, compositional homogeneity, and densification, 2) Crystallization vs. composition subsequent to pyrolysis, 3) High temperature phase partitioning of metastable structures produced during crystallization after pyrolysis, 4) Grain growth phenomena as related to different binary, solid-solution cations and composition with different binary systems, 5) Microstructural instabilities of polycrystalline thin films, 6) Microstructural instabilities of polycrystalline fibers constrained by composite matrices, 7) Formation of single crystal thin films as a function of differential composition and lattice mismatch, and 8) Relations between processing flaws and strength for fibers produced by dry spinning. The pertinent results of these studies and their interrelations are summarized.

14. SUBJECT TERMS	15. NUMBER OF PAGES
Ceramic Microstructures, ZrO_2 Binary Systems, Precursors	58
	16. PRICE CODE

17. SECURITY CLASSIFICATION OF REPORT	18. SECURITY CLASSIFICATION OF THIS PAGE	19. SECURITY CLASSIFICATION OF ABSTRACT	20. LIMITATION OF ABSTRACT
Unclassified	Unclassified	unclassified	UL

Final Report Report

15 June, 1987 through 15 June, 1990

Grant: AFOSR-87-0291

Partitioning Reactions to Control and Develop Unique Microstructures

September 15, 1990

Submitted to

Department of the Air Force
Air Force Office of Scientific Research
Electronic and Material Sciences
Bolling Air Force Base, DC 20332-6448

Submitted by

Materials Department
College of Engineering
University of California, Santa Barbara
Santa Barbara, CA 93106

Principal Investigator: F. F. Lange, Prof. of Materials

1. Background

This research program concerned precursors to ceramics and unique microstructures and structures formed from such precursors. Liquid precursors can form useful structures: small spheres (for particles), fibers (for composites, communication, etc), and thin films (for coatings, electronic ceramics, etc). Today, nearly all advanced ceramics are produced by some chemical route that initiates with either a solid (precipitated hydroxide, etc) or liquid (soluble alkoxide, acetate, metal-organic polymers, etc) precursor. In all cases, the single phase ceramics are produced by a low temperature pyrolysis, viz., decomposition to a gas plus a solid ceramic, followed by a high temperature heat treatment.

Research was initiated by investigating the high temperature stability of binary ZrO_2 microstructures produced from mixed Zr-acetate + metal nitrate liquid precursors. These binary systems are not only unique because of their ability to produce ceramics with very high fracture resistance due to stress-induced transformation toughening (and possibly, ferroelastic domain switching), but also because they produce a unique, fine grained ceramic in which grain growth is extremely sluggish for extended periods at temperatures where powder compacts are densified.

Our studies include: 1) Liquid precursor formulation, pyrolysis, compositional homogeneity, and densification, 2) Crystallization vs composition subsequent to pyrolysis, 3) High temperature phase partitioning of metastable structures produced during crystallization after pyrolysis, 4) Grain growth phenomena as related to different binary, solid-solution cations and composition with different binary systems, 5) Microstructure instabilities of polycrystalline thin films, 6) Microstructural instabilities of polycrystalline fibers constrained by composite matrices, 7) Formation of single crystal thin films as a function of differential composition and lattice mismatch, and 8) Relations between processing flaws and strength for fibers produced by dry spinning. The pertinent results of these studies and their interrelations will be summarized in the next section.

Since initiating this program, we have recognized two phenomena of critical scientific and technological importance to binary ceramics produced from precursors. First, since crystallization occurs at relatively low temperatures, atomic mobility is kinetically limited and thus, the crystal structure formed during pyrolysis can be metastable. That is, crystallization lowers free energy,

but the chemical composition is frozen into a structure that may not exist at higher temperatures where partitioning into different structures with equilibrium compositions can occur. The metastable structure formed during pyrolysis can be predicted with knowledge of kinetic-limited phase relations, a subject developed to explain metastable structures observed during the rapid solidification of metal alloys.

Second, phase partitioning during heating is different than conventional phase partitioning phenomena that occur during cooling, after high temperature processing (e.g., crystallization from melts and precipitation within solids). For example, since the free energy change associated with partitioning is measured from the low temperature, metastable structure formed during pyrolysis, both nucleation and growth rates increase with temperature. This is different for conventional partitioning (during cooling) where the differential free energy is associated with a high temperature phase, viz., nucleation rate increases during cooling and growth rates are greatest at higher temperatures. In addition, partitioning after pyrolysis and crystallization occurs within a low density network formed with partially sintered, nanometer crystallites. Conventional partitioning occurs within dense systems, viz., within melts and solids.

2. Summary of Research

2.1 Zr-Acetate Precursors - Pyrolysis and Densification

Zirconium acetate is commercially available as an inexpensive, aqueous solution that contains an equivalent of 20-22 wt % ZrO_2 (precisely determined by TGA). The solution is describe in chemical handbooks as containing complexed, partially hydrated acetate molecules that link together during solvent evaporation. It is also described by one manufacturer as a ZrO_2 sol. Its viscosity increases dramatically as the equivalent ZrO_2 content approaches ≈ 50 wt % during evaporation, and it forms a 'solid-like', amorphous gel at an equivalent ZrO_2 content of ≈ 55 wt %. Its rheological and 'solid-like' gel characteristics are similar to other liquid precursor chemistries (other acetates, citrates, nitrates, oxyclorides, partially hydrolized alkoxides, etc) to ceramics. These characteristics allow liquid precursors to be atomized to droplets (for powders), formed as thin films on substrates by either spin coating or dipping, and dry spun as fibers.

During heating, the 'solid-like' gel first loses its water at temperatures < 150 °C (TGA) which is characterized by an endothermic reaction (DTA) centered at 80 °C. Once heated to 200 °C, the solid precursor is non-hydroscopic and does not redissolve in water. The major weight loss occurs between 200 and 400 °C where the solid precursor pyrolyzes to ZrO_2 plus residual, free carbon. The free carbon is lost by oxidation, characterized by an exothermic reaction centered at ≈ 800 °C. Crystallization of ZrO_2 occurs subsequent to pyrolysis, characterized by an exothermic reaction centered at 450 °C which is not associated with a weight loss. Preliminary TEM observations suggests that crystallization may initiate during pyrolysis. After heat treatments between 400 and 800 °C, the structural form (tetragonal vs cubic) of the crystalline ZrO_2 is difficult to determine because of the broad cubic-like diffraction peaks produced by the small (< 20 nm at < 800 °C) size of the primary ZrO_2 crystallites.

Binary (and ternary) ZrO_2-metal oxide compositions can be formed by mixing appropriate, water soluble metal salts with either as received or concentrated Zr-acetate solutions. After drying, amorphous (determined by XRD) solid precursors can be formulated containing up to the equivalent of 40 mole % Y_2O_3 or MgO (based on the ZrO_2 content) with metal nitrate additions. Many other binary systems have also been formulated in our studies. These observations show that the nitrates do not phase separate during drying by crystallization, and suggests that the binary cations are mixed at the molecular scale*. The analytical TEM was used to determine spatial compositional variation after the 'solid' precursors were rapidly heated to 800 °C to produce a solid with a mean crystallite size of ≈ 20 nm. Figure 1 shows the equivalent Gd_2O_3 content is nearly identical for each of the 150 nm areas analyzed, and nearly identical, within statistical counting error (± 0.1 mole %), to the formulated composition (either 1 or 3 mole % Gd_2O_3). Thus, all current evidence strongly suggests that the binary cations are mixed at least to the scale (150 nm) observed in Fig. 1.

---

* Preliminary observations suggest that phase separation can be accomplished by increasing the pH with additions of a base; basic conditions cause hydroxide precipitation which transforms the solution to low density, sol-gel.

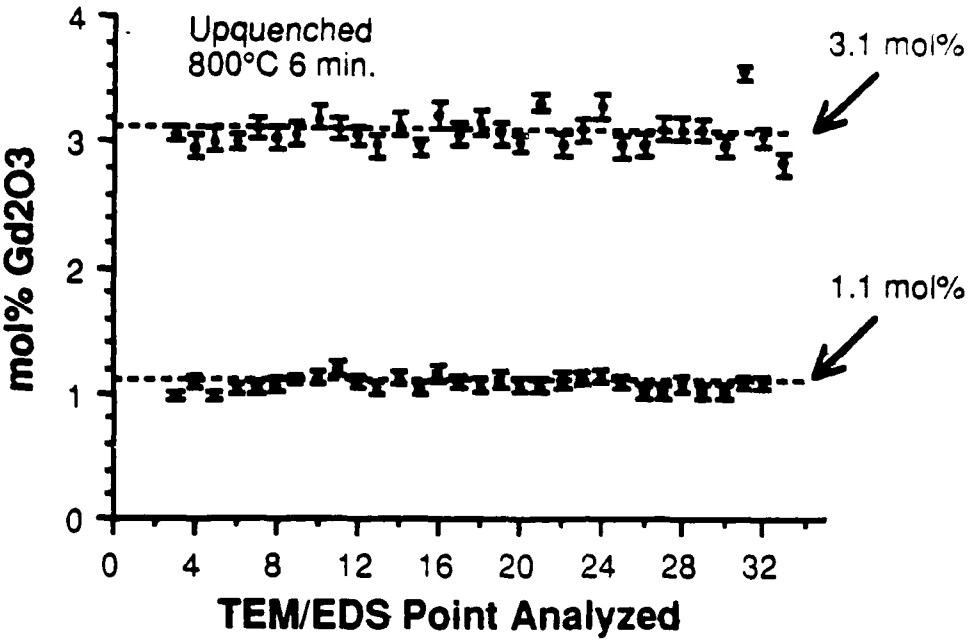

Figure 1 Equivalent Gd_2O_3 content in two precursor compositions (ZrO_2 + either 1 or 3 mole % Gd_2O_3) heat treated at 800 °C vs area (150nm) examined with TEM/EDX to show compositional uniformity.

Figure 2 illustrates the densification behavior of the Zr-acetate precursor containing an equivalent of 3 mole % Y_2O_3 determined by measuring the shrinkage of continuously spun fiber segments, incrementally heated to 1300 °C on a single crystal Al_2O_3 substrate. The data is plotted relative to the theoretical density of tetragonal ZrO_2 containing 3 mole % Y_2O_3. As shown, although the major change in density occurs during and subsequent to pyrolysis (between 200 and 800 °C), a large change occurs as the precursor gel losses its water (< 200 °C), and a smaller change occurs with the oxidation of free carbon (> 800 °C). Densification appears complete between 1200 and 1300 °C. It should be noted here that the shrinkage associated with lose of water from the solid-like gel can result is the major cause of damage in fibers and thin films. Constraint of this shrinkage during the heat treatment of fibers causes continuous fibers to break into fragments, and produces residual cracks in these fragments. Shrinkage of thin films during drying is also constrained by their substrate resulting in cracking when the film thickness is greater than a critical value.

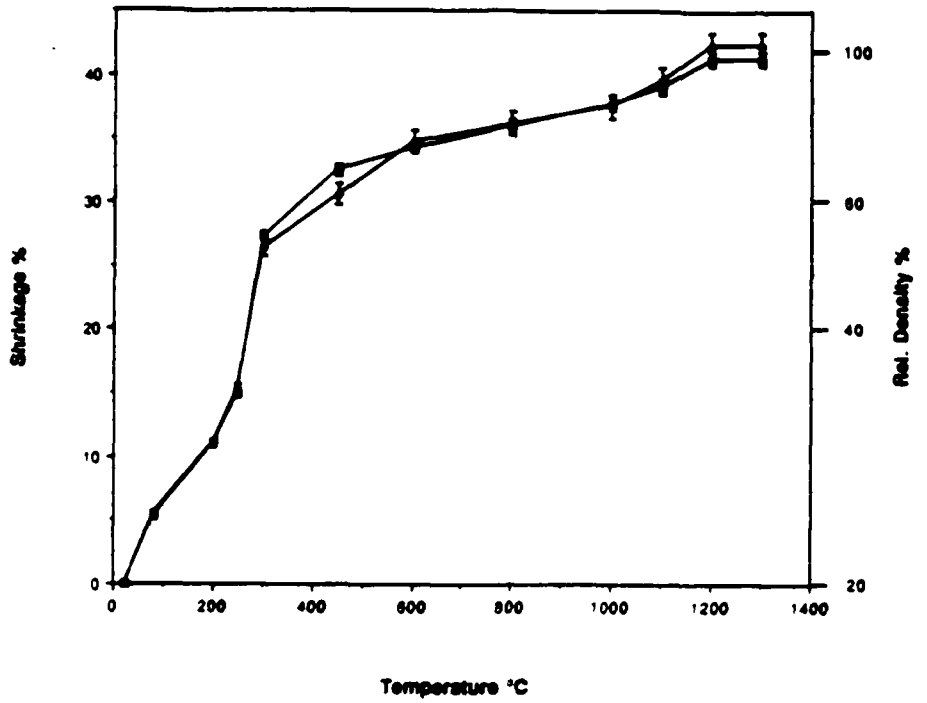

Figure 2 Densification behavior of the Zr-acetate precursor containing an equivalent of 3 mole % Y_2O_3 determined by measuring the shrinkage of continuously spun fiber segments, incrementally heated to 1300 °C on a single crystal Al_2O_3 substrate.

2.2 Crystallization vs Composition

As summarized above, crystallization of the ZrO_2 solid-solution compositions occur at low temperatures (400-500 °C) just subsequent (or concurrent) to pyrolysis. For two different binary systems, viz., ZrO_2-Gd_2O_3 and ZrO_2-MgO, we have shown that the structures produced during crystallization systematically depend on composition; similar, preliminary data also exists for several other systems. The data show that when the concentration of the solid-solution cation is less than a critical value ($C < C_o$), the binary composition crystallizes with the tetragonal structure. And, when the concentration of the cation is greater than a critical value ($C > C_o$), the composition crystallizes with the cubic structure. For the ZrO_2-Gd_2O_3 system, C_o = 6 to 7 mole % Gd_2O_3 and C_o = 8 to 9 mole % MgO for the ZrO_2-MgO system. The uncertainty in the exact value of C_o is due to: a) the diffraction patterns for the two structures are nearly identical as the composition approaches C_o and b) the small size of the crystallites

produced after pyrolysis cause significant peak broadening.

As discussed in the next section, detailed work for the ZrO_2-Gd_2O_3 system (and work by others for many other binary systems) would not predict the crystallization of a single structure, nor the crystallization of the observed structures. Namely, conventional phase diagrams show that nearly all the formulated compositions would lie within a two phase region and thus, would predict the concurrent crystallization of two structures (e.g., either monoclinic + cubic, or tetragonal + cubic). We now recognize that our results (and those of others) can be simply interpreted with the use of concepts developed for kinetically limited phase equilibria.

The concept of kinetically limited crystallization was primarily developed to explain the apparent, non-equilibrium crystallization during rapid solidification of molten metals. It is based on the premise that diffusion does not occur during crystallization. With this premise, one reinterprets equilibrium phase relations with respect to the free energy of crystalline structures and not with respect to compositional equilibrium considerations. Figure 3 schematically illustrates the free energy of the tetragonal and cubic structures of ZrO_2, at some temperature, as a function of solid-solution metal oxide concentration. The minimum free energy for each curve is equilibrium composition (C_t and C_c) for each of the two structures. These values represent the equilibrium phase boundaries for a two phase region. At true equilibrium (kinetically unlimited), any composition

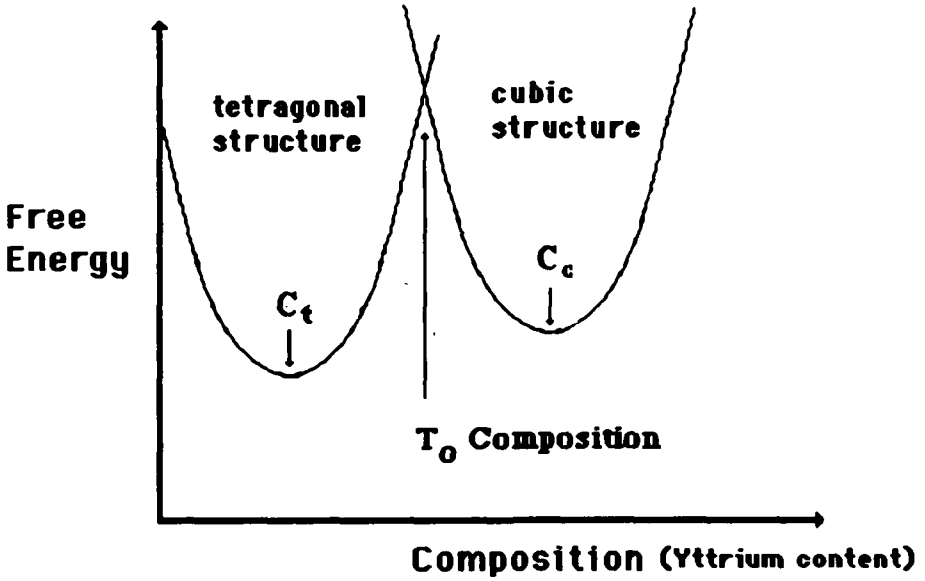

Figure 3 Schematic illustration of the free energy of the tetragonal and cubic structures of ZrO_2, at a given temperature, as a function of solid-solution metal oxide concentration.

between these two equilibrium compositions should consist of two phases (tetragonal + cubic), each with their specific, equilibrium composition. For the case where crystallization occurs without compositional equilibration (kinetic limited) any composition between the two equilibrium compositions will crystallize with one of the two structures, viz., the structure will be tetragonal for $C < T_o$ and cubic for $C > T_o$. The free energy for both structures is identical at T_o. The compositions C_t, C_c and T_o are temperature dependent. Conventional (kinetic unlimited) phase diagrams represent C_t and C_c vs temperature as phase boundaries. Since $C_t < T_o < C_c$, the temperature and compositional dependence of C_o can generally be estimated by a line that divides the two phase region as shown in Fig. 4 for the ZrO_2-MgO binary system; the T_o boundary can extend to room temperature. Experimentally, T_o is determined by characterizing the structure that crystallizes under conditions of kinetically limited diffusion as a function of composition.

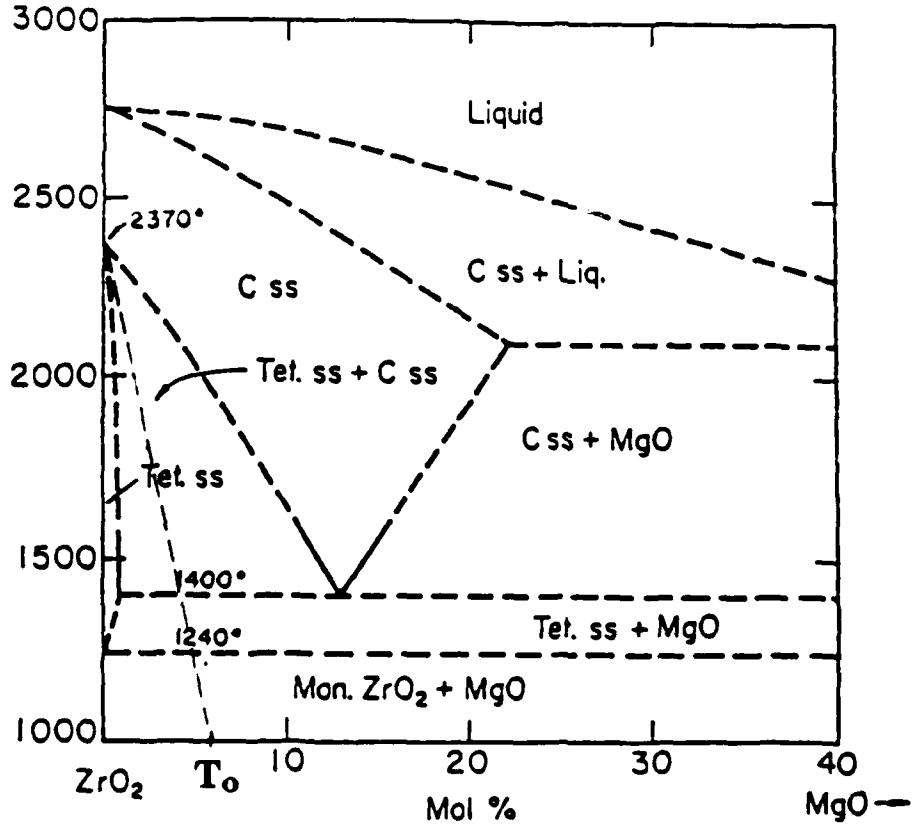

Figure 4 T_o compositions vs temperature, where metastable compositions with the tetragonal and cubic structures have the same free energy, superimposed on the equilibrium phase diagram for the ZrO_2-MgO binary system.

The concept and use of kinetic limited phase equilibria certainly applies to the low temperature crystallization that occurs after (or during) ceramic precursor pyrolysis. For the case of ZrO_2-metal oxide binary systems, the equilibrium, two phase field (tetragonal + cubic) only exists at high temperatures, yet, the T_o compositional boundary in a kinetically limited phase diagram will extend to very low temperatures. Thus, the kinetically limited phase diagram (which can be estimated from the convensional equilibrium phase diagram) can be used to predict the crystal structure that forms during ceramic precursor pyrolysis. For the case of the two systems studied, ZrO_2-Gd_2O_3 and ZrO_2-MgO, T_o was experimentally determined as 6 to 7 mole % Gd_2O_3 and 8 to 9 mole % MgO, respectively. Although these XRD determinations were carried out after the compositions were heated to $\geq$ 800 °C (larger crystallites had to be developed for XRD determinations), all evidence suggest that values of T_o are representative for the crystallization temperature (400-500 °C). Consistent with kinetic limited phase equilibria, at $C < T_o$ the tetragonal structure is observed, whereas the cubic structure is observed for $C > T_o$.

The use of kinetic limited phase equilibria for ceramics produced from precursors has many significant implications. First of all, it is interesting to note that although the use of kinetic limited phase equilibria has been under study for many years in the context of rapid solidification, it has not been applied to ceramic precursor crystallization despite numerous studies of ceramic synthesis from such precursors. The literature is filled with studies in which 'non-equilibrium' structures and compositions are produced during low temperature ceramic synthesis. Other implications will be discussed below.

2.3 High Temperature Phase Partitioning

One important implication of crystallization under kinetic limited conditions is that the metastable structure(s) produced at low temperatures will partition into equilibrium structures and compositions at higher temperatures. This partitioning has significant implications concerning ZrO_2 binary systems. Namely, all binary powders (e.g. ZrO_2 + Y_2O_3) that are formulated and manufactured to produce ceramics that exhibit stress-induced transformation toughening are produced from precursors (usually zirconium oxychlorides) that crystallize during calcination under kinetic limited conditions. Our studies show

that partitioning at temperatures (1400 °C) where these powders are densified is very sluggish, and thus the dense, polycrystalline materials are still metastable compositions. The importance of this will be review after a discussion of our partitioning study.

Our partitioning studies involved several different ZrO_2 binary systems. For most, XRD and limited analytical TEM was used to follow partitioning kinetics at 1400 °C. The ZrO_2-Gd_2O_3 system was chosen for detailed study with high resolution, energy dispersive spectroscopy (TEM/EDS). We used the ZrO_2-Gd_2O_3 system for the TEM/EDS study because the Gd-Lα peak could be easily distinguished from the Zr-Lα peak, whereas, the high intensity Y-Lα peak overlaps the Zr-Kα peak. Otherwise, data strongly suggest that both binary systems exhibit similar partitioning kinetics. For this study, TEM specimens of ZrO_2 + 3 mole % Gd_2O_3, formulated from acetate + nitrate solutions, were prepared after pyrolysis and heat treatment for different periods (up to 500 hr) at 1400 °C. The Gd/Zr ratio (and the equivalent Gd_2O_3 mole %) was determined for a large number of grains (grain size > 300 nm) for each heat treatment with a probe size of 150 nm. Since the probe size was smaller than the grain size, the Gd distribution within the grains could also be determined. Synthetic standards were used to calibrate the Gd/Zr ratio and relate the ratio to mole % Gd_2O_3 within the grains. In addition, sufficiently long counting periods were used to determine the Gd content with a precision of ± 0.1 mole % Gd_2O_3.

The results of the ZrO_2-Gd_2O_3 TEM/EDS partitioning studies are shown in Fig. 5, illustrating that the grains can be classified into two groups, one group with an average Gd_2O_3 content that initiates at the formulated composition (3 mole % Gd_2O_3) which decreases as a function of heat treatment time, and a second group that contains 8 mole % Gd_2O_3 which remains constant with increasing heat treatment period. Grains in the first group (lower and decreasing Gd_2O_3 content) crystallize subsequent to pyrolysis with the tetragonal structure with a non-equilibrium composition due to kinetic limited considerations. During the initial heat treatment periods, the Gd content within each tetragonal grain and from grain to grain can be different by as much as 1 mole % Gd_2O_3. Grains in the second group (high and constant Gd_2O_3 content) are cubic; these grains are produced during phase partitioning and very few grains, large enough to be observed much less measured, are found during the initial heat treatment period. During the heat treatment, the cubic grains grow to a much larger size relative to the smaller tetragonal grains.

The data in Fig. 5 shows that the tetragonal phase produced after pyrolvsis under kinetic limited conditions is certainly a metastable phase. These data define the boundaries of the two phase field at 1400 °C. After apparent compositional equilibrium (200 hr), Fig. 5 shows that the maximum solid-solubility of Gd_2O_3 in the tetragonal structure is 1.0 ± 0.1 mole %, and that the tetragonal + cubic phase field extends from 1.0 ± 0.1 to 8.0 ± 0.1 (the mole % of Gd_2O_3 in the cubic grains) mole % Gd_2O_3. After the composition containing 3 mole % Gd_2O_3 is fully partitioned, it contains a continuous network (≈ 30 volume %) of cubic grains within a matrix of tetragonal grains.

Although our data and observations clearly show that the metastable grains slowly lose Gd and that cubic grains develop and grow larger as they receive Gd, the mechanism responsible for phase partitioning is not understood. Typically, when a composition is cooled from a higher temperature into a two phase region, partitioning occurs by precipitation, i.e., precipitates develop and grow both within grains and on grain junctions (their positions of lowest free energy). Although we do find strong compositional differences within ZrO_2 grains, we currently have no evidence that these compositional differences are related to precipitates, nor do we observe precipitates at grain junctions. Preliminary results concerning the distribution of Gd within materials heat treated at lower temperatures strongly suggest that phase partitioning begins at lower temperatures and depends on the heating rate to the desired temperature. These results strongly suggest that partitioning begins when the ZrO_2 grains are much smaller than those studied at 1400 °C (e.g., ≈ 20 nm at 800 C vs ≈ 300 nm after 1 hr at 1400 °C). Thus, small cubic grains (or precipitates) are expected to develop during low temperature partitioning before larger grains are observed at 1400 °C. Understanding and exploiting this phase partitioning mechanism will be one of the major proposed research efforts.

Figure 5 shows that partitioning at 1400 °C is very sluggish, viz., partitioning appears complete after 200 hrs, whereas powders used to form dense polycrystalline bodies are generally densified at this temperature for only 1 to 2 hours. These results and less detailed results previously obtained for the ZrO_2-Y_2O_3 system clearly show that the materials densified with commercial powders are metastable tetragonal compositions that are not fully partitioned. Since both the spontaneous (during cooling) and stress-induced (during crack extension) tetragonal to monoclinic transformation depends on the Y_2O_3 (or Gd_2O_3) content of the tetragonal phase, the ease in which this transformation takes place will

depend on the amount of phase partitioning and thus the period at the processing temperature. Likewise, the nucleation of this transformation can take place from regions of lower Y_2O_3 (or Gd_2O_3) content within individual grains. In the past, it was proposed that the retention of the tetragonal toughening agent and its ease for stress-induced transformation (as well as its contribution to fracture toughness) was only dependent on grain size. Our results clearly show that phase partitioning, i.e., period at the processing temperature, is a significant issue concerning both the retention of the tetragonal toughening agent during processing, its transformation mechanics, and its contribution to fracture toughness.

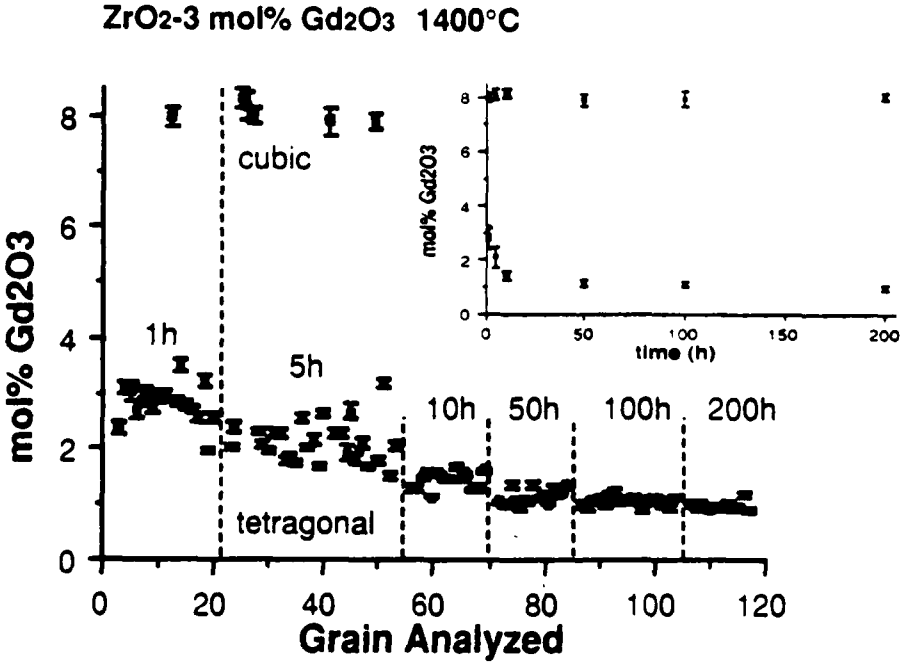

Figure 5 TEM/EDS results of different grains analyzed for a ZrO_2 composition containing 3 mole % Gd_2O_3 heat treated at 1400 °C for periods up to 500 h. The Gd_2O_3 content in the tetragonal grains decreases over this period, while larger cubic grains containing 8 mole % Gd_2O_3 emerge.

2.4 Grain Growth in Different ZrO_2 Binary Systems

As indicated in the introduction, certain compositions within different ZrO_2 binary systems are unique, relative to other ceramics, due to their sluggish grain growth kinetics and the fine grained microstructures they produce after prolonged periods at temperatures that produce dense bodies from powders. One of the goals of our current work is to characterize this grain growth phenomena with respect to composition, different binary systems, and other phenomena concurrent with grain growth. As indicated below, all of our results are not consistent with any currently proposed mechanism.

Figure 6 illustrates that grain size of a ZrO_2 + 3 mole % Y_2O_3 composition heated to a temperature between 1000 and 1500 °C at 5 °C/min. and immediately cooled. As shown, the average grain size increases by more than an order of magnitude over this temperature range, viz. from ≈ 50 nm to ≈ 500 nm. The period over which this grain growth occurs is 100 minutes ([1500 °C - 1000 °C] /[5 °C/min] = 100 min.), resulting in a grain growth rate of ≈ 4.5 nm/min. As shown

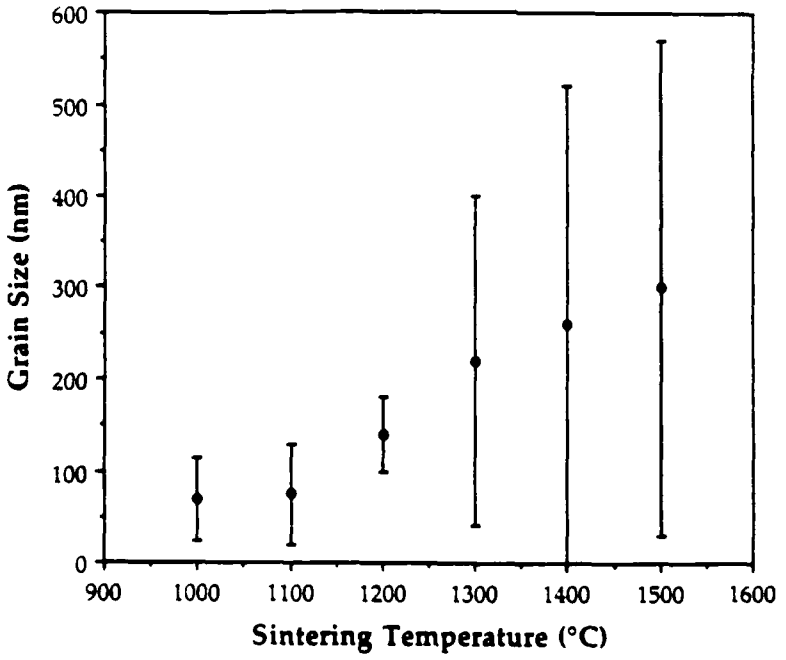

Figure 6 Grain size of a ZrO_2 + 3 mole % Y_2O_3 composition heated to a temperature between 1000 and 1500 °C at 5 °C/min. and immediately cooled.

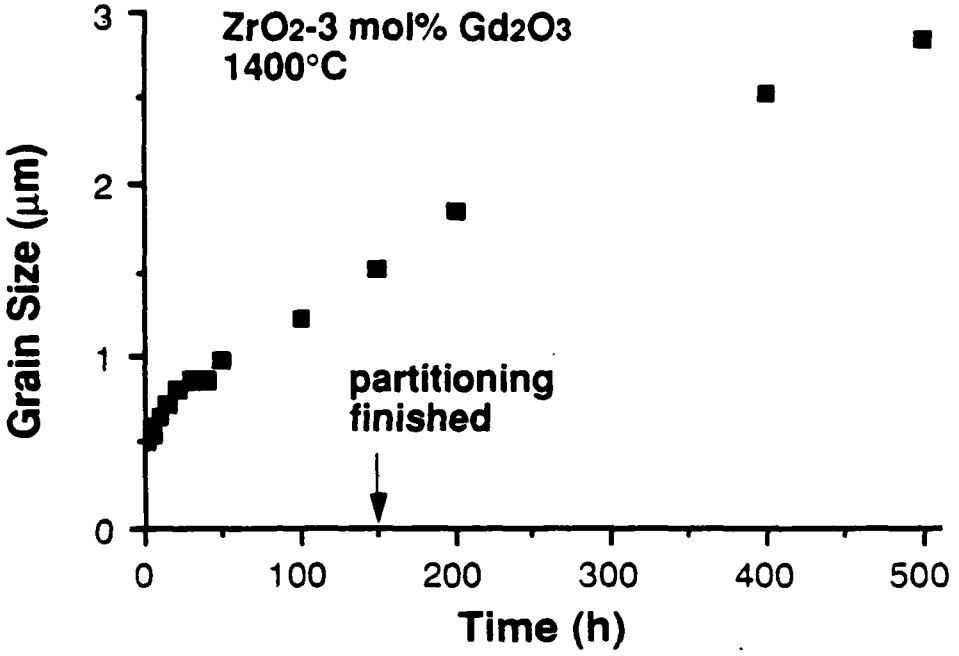

Figure 7 Grain size for a ZrO_2 + 3 mole % Gd_2O_3 composition heated to 1400 °C for periods up to 500 hrs.

in Fig. 2, the material does not fully densify until 1200 to 1300 °C, suggesting that some of this grain growth is inhibited by residual porosity. In contrast, Fig. 7 illustrates the grain growth kinetics for a ZrO_2 + 3 mole % Gd_2O_3 composition heated to a temperature of 1400 °C for periods up to 500 hrs (grain size increased from ≈ 500 nm to ≈ 3000 nm) which exhibits a significantly slower grain growth rate of ≈ 0.08 nm/min. Nearly identical results are obtained for a previously characterized ZrO_2 + 3 mole % Y_2O_3 composition made with commercial powder. These data show that grain growth is approximately 50 time faster during heating to 1400 °C relative to the grain growth that occurs when the material is held at 1400 °C for extended periods.

Figure 8 illustrates the grain size vs composition, after 1 hr at 1400 °C, for a series of compositions within the ZrO_2 rich portion of the ZrO_2-Gd_2O_3 system. As reviewed above, all compositions up to between 6 to 7 mole % Gd_2O_3, crystallize with the tetragonal structure after pyrolysis, whereas the equilibrium two phase (tetragonal + cubic) field lies between 1 and 8 mole % Gd_2O_3. Similar, but less extensive results have been previously reported for the ZrO_2 rich portion of the

ZrO_2-Y_2O_3 system. Figure 8 shows that compositions within the equilibrium, two phase field have the smallest grain size and that the grain size decreases with increasing Gd_2O_3 content between 0 and 1 mole %.

As detailed in Tech. Rept No. 6, the grain growth phenomena of selected portions of different ZrO_2-MO (M = Ca^{+2}, Nd^{+3}, Gd^{+3}, Y^{+3}, In^{+3}, Dy^{+3}, and Ce^{+4}) systems were examined. In general, grain growth behavior for all systems resemble those shown in Figs. 6-8, viz., a) grain growth was rapid as the composition was heated to 1400 °C, b) grain growth was sluggish at 1400 °C, and c) grain size (1 hr, 1400 °C) decreased as the composition entered the two phase field, and was smallest within the two phase field. No significant differences in grain growth phenomena were observed between binary systems with either di- or trivalent cations, viz., grain growth behavior vs composition and time appeared nearly identical regardless of valence state and cation size. Compositions containing CeO_2, produced similar behavior except that grain growth was more rapid relative to any other system.

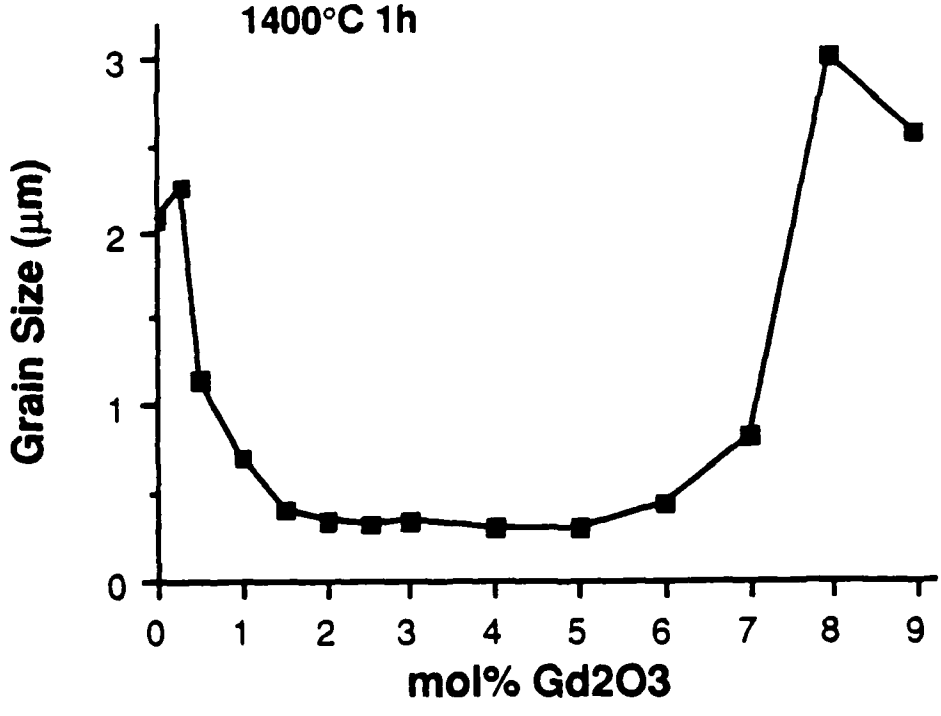

Figure 8 Grain size vs composition, after 1 hr at 1400 °C, for a series of compositions within the ZrO_2 rich portion of the ZrO_2-Gd_2O_3 system. Compositional field corresponding to smallest, compositional independent grain size corresponds to two phase (tetragonal + cubic) field when compositions equilibrate (≈ 150 hrs).

Three different models have been proposed to explain the sluggish grain growth behavior found in the ZrO_2-metal oxide binary systems. Based on observations for several compositions in the ZrO_2-Y_2O_3 system, Theunissen et al[1] suggested that equilibrium segregation of Y_2O_3 occurs at grain boundaries that limit grain boundary motion due to solute drag considerations. More recently, Huange and Chen [2] suggest a similar mechanism, but, in addition, suggest that the effect of solute drag will depend on the valence state of the segregating cation, viz., they suggest a space-charge drag model. Based on large compositional differences from grain to grain produced during phase partitioning, Lange et al[3] suggested that grain growth was hindered because lattice strains would arise unless compositional changes could accompany boundary motion. Currently, none of these models appear consistent with all observations.

The solute drag and solute induced space-charge drag models are certainly appealing, but neglect the observations that grain growth is severely hindered even when a silicate liquid is present at all grain junctions, i.e., when grain boundaries do not exist. In addition, these models neglect that the compositions under study are metastable, require long periods to reach equilibrium through phase partitioning, and that observed segregation may be due to phase partitioning. The lattice strain model requires that compositional differences, e.g., those produced during phase partitioning as discussed above for the ZrO_2-Gd_2O_3 system, produce different lattice parameters. Our work, relating grain growth phenomena to the compositional dependence of lattice parameters, has shown that sluggish grain growth can occur in the ZrO_2-In_2O_3 system, but In^{+3} does not sufficiently change the lattice parameters of tetragonal ZrO_2 (the ionic size of In^{+3} and Zr^{+4} are nearly identical). We thus conclude that the lattice strain model does not explain the unique grain growth phenomena in two phase compositional regions of ZrO_2-metal oxide systems.

2.5 Instabilities Due to Grain Growth During Constrained Shrinkage (Thin Films and Fibers)

We have shown that polycrystalline thin films, constrained by their substrate, and fibers, constrained by a matrix material, break-up into isolated grains during grain growth. The thin films and fibers used in these studies were produced with the same liquid precursors described above. As detailed in

Technical Repts. 2 and 3, it was shown that these morphological instabilities occur when the gain size to film thickness (or fiber diameter) ratio exceeds a critical value. For both cases, it was concluded from a thermodynamic analysis that the break-up phenomena is a continuous event that lowers the free energy of the system caused by the disappearance of grain junctions as surfaces and interfaces achieve equilibrium configurations under conditions of constrained shrinkage. If unconstrained, both the films and fibers would shrink, instead of breaking up, to maintain a equilibrium balance between grain boundary and interfacial energies. Our thermodynamic analyses not only explains these morphological instabilities, but also were organized as equilibrium configuration diagrams to predict the grain size required to cause the break-up phenomena as a function of the different interfacial energies.

These results are of significant interest for the processing and use of composite systems at high temperatures. Fibers are coated to protect them from matrix reactions and/or to produce desirable interfacial fracture phenomena. Such coatings can undergo the same morphological instability described above if the grain size to coating thickness exceeds a critical value. Likewise, polycrystalline fibers can undergo the same morphological instability during either composite processing or use, if the grain size to fiber diameter exceeds a critical value. These instabilities are now understood, can be predicted, and can be avoided by controlling grain growth.

In addition, it has recently been observed that the same instabilities observed for thin films and fibers are also observed within the sintering matrix powder during the pressureless densification of composite systems. Constraint of shrinkage due to the reinforcement network causes partially dense regions to form larger pores that limit the end-point density of the composite system.

2.6 Single Crystal Thin Films From Liquid Precursors

Single crystal ZrO_2-metal oxide thin films have been produced by spin coating cubic, single crystal ZrO_2 (+9.5 mole % Y_2O_3) substrates with (100) orientation. As detailed in Tech. Rept. No. 5, a report of preliminary results for an MRS meeting, Zr-acetate + Y-nitrate liquid precursor compositions ranging from 0 to 40 mole % Y_2O_3 produced the following results: a) polycrystalline, but strongly (100) oriented films (composition: 25 m/o Y_2O_3) were observed after pyrolysis at 500 °C, b) electron back-scattering channeling patterns (SEM) showed

that film compositions ranging between 3 to 20 m/o Y_2O_3 where epitaxially oriented with respect to the substrate at 1100 °C, whereas, c) XRD showed that only the compositions ranging between 6 to 15 m/o Y_2O_3 did not indicate any polycrystallinity at 1100 °C.

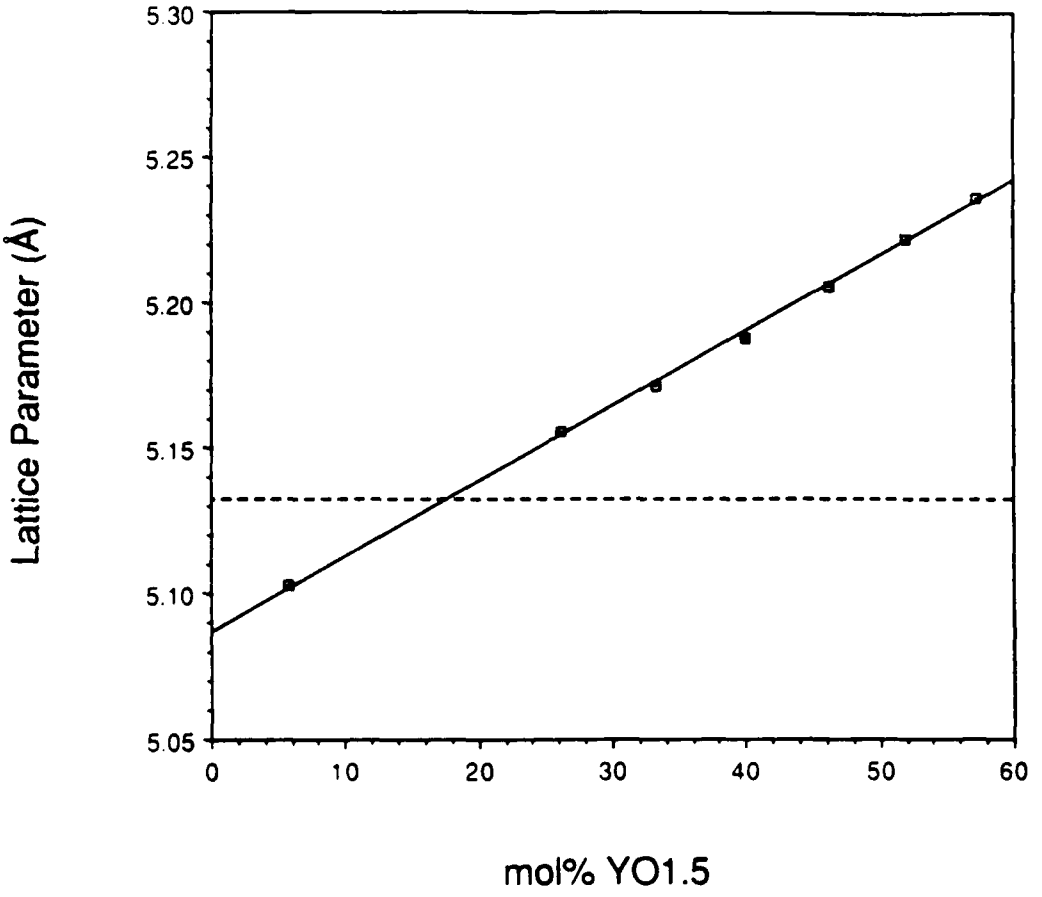

Figure 9 Lattice parameter of ZrO_2 solid-solution, single crystal thin films vs $Y_{1.5}O$ content prepared by heat treating precursor composition, spun onto a cubic single crystal of ZrO_2 (+ 9.5 mole %Y_2O_3), at 1400 °C.

Recent results have shown that compositions between 3 to 40 m/o Y_2O_3 fully form single crystal thin films after short periods at 1400 °C. Over this compositional range, the thin film was a single crystal with the cubic structure and, as shown in Fig. 9, a lattice parameter consistent with its composition, but different from its underlying, cubic substrate. These results show that little, if any, interdiffusion has occurred during these heat treatments. In addition, these data show that epitaxially related thin films can be formed, using liquid precursor routes, with lattice mismatch strains up to 1.5%, and that epitaxially

related films can be produced at lower temperatures when the lattice strain is < ± 0.5 %. It should be noted that the data shown in Fig. 9 strongly suggests that the composition containing 3 m/o Y_2O_3 exhibits an apparent cubic structure, whereas, without the substrate, these same compositions crystallize with the tetragonal structure as predicted with kinetic limited phase equilibria. These preliminary results suggest that an epitaxial related substrate can over-ride the more thermodynamic stable structures predicted with kinetic limited phase equilibria.

Recent studies have concentrated on determining how the precursor thin film develops its epitaxial relation and on characterizing the microstructural changes that occur during heat treatment as detailed with planar and cross-sectioned specimens prepared for TEM. Planar specimens of thin films containing 25 m/o Y_2O_3 show that the thin film is a single crystal near the substrate interface at 900 °C and that a dislocation network develops at the film-substrate interface between 1300 to 1400 °C as shown in Fig. 10. This network apparently accommodates some of the lattice mismatch. Since the dislocation network is not observed at 1300 °C, it appears that some diffusion is required for its formation.

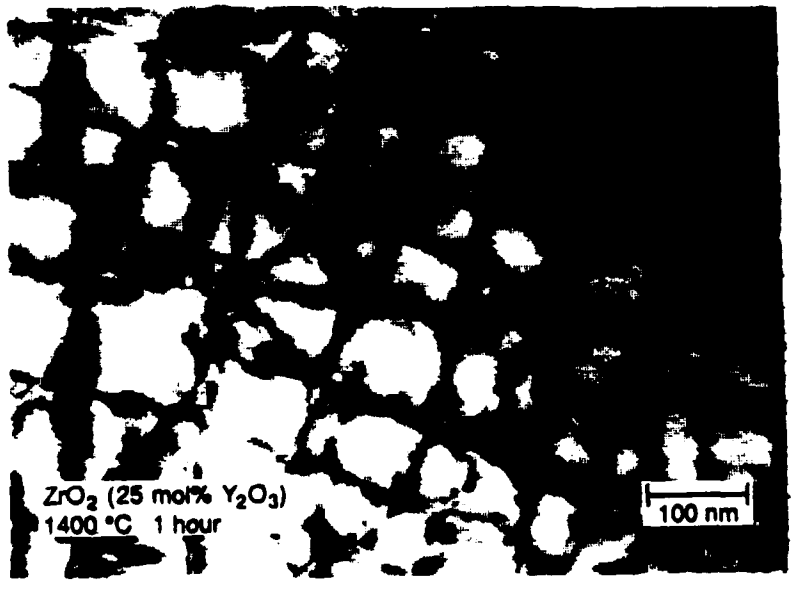

Figure 10 Dislocation network developed at the interface between a single crystal thin film (ZrO_2 + 25 mole %Y_2O_3) epitaxially produced at 1400 °C on a single crystal substrate (ZrO_2 + 9.5 mole %Y_2O_3). Most dislocations have a [110] trace.

Besides the technological implications of this work, the results to date show that a significant understanding of the science associated with a) precursor crystallization as influence by epitaxial surfaces, b) interface structure vs lattice mismatch, and c) the determination of cation diffusion coefficients can be gained in these studies. These scientific implications will be detailed below.

2.7 Spinning of $Zr(Y)O_2$ Fibers: Flaw Populations and Processing

Continuous precursor fibers were produced by dry spinning a liquid Zr-acetate + Y-nitrate solution containing 1 wt % polyethylene oxide (PEO) (MW = 5,000,000). Dense, polycrystalline, tetragonal fibers (5 to 10 μm diameter) containing 3 m/o Y_2O_3 where produced after pyrolysis and heat treatment at 1300 °C with an average tensile strength of 2.3 GPa. The goals of this research were to understand how liquid precursors can be spun into fibers (work in this area is not reported in the open literature due to proprietary industrial concerns), and specifically, to understand how flaw populations, which limit fiber strength, are introduced during processing. Knowledge of how flaws are related to processing will lead to processing changes and stronger fibers. Prof. P. Smith (UCSB-Materials Dept., Polymer Group) and Dr. David Marshall (Rockwell International Science Center) are contributors to this work.

This work has shown that although a sufficiently concentrated Zr-acetate (+nitrate) solution could be spun into fibers without PEO additions, the solution was too concentrated to allow reliable spinning. Namely, since the spinnable concentrated solution was well beyond its gel point, small changes in the water content would cause the solution near the spinneret to harden. Studies showed that an addition of 1 wt % PEO (MW = 5,000,000) to a solution containing an equivalent of 50 wt % ZrO_2 was required to produce sufficiently high elongation viscosity to produce a stable liquid jet which would dry to a solid-like gel prior to spooling. This amount of PEO was approximately 20 times the critical concentration required to produce an interconnected polymer network. Higher contents would have been required for a polymer with a lower molecular weight.

Once the spinability of precursor fibers was established, processing conditions were related to tensile strength. All fracture surfaces were observed in the SEM in a attempt to recognize the strength limiting flaw and its relation to processing. Since pyrolysis and densification was not accomplished during

continuous fiber spinning, fiber bundles cut from the spool were heat treated under different conditions.

It was established that the most critical processing step occurred as the water was removed from the solid-like gel at temperatures < 200 °C. Any constraint to the ≈ 8 to 10 % linear drying shrinkage (see Fig. 2) would cause the fiber to fragment. Drying the fibers on a flat surface, in bundles, and between supporting rods produced sufficient shrinkage constraint to cause fragmentation. In addition, although the fragments were sufficiently long enough for tensile strength determinations, they still contained partial cracks which contributed to a large scatter in strength values (0.1 to 3 GPa) and a mean strength of only ≈ 1 GPa. These partial cracks could be observed in the precursor fiber under oblique illumination, and on the fracture surface after heat treatment and strength determination.

Constraint to shrinkage during drying was avoided by designing a spool with a variable diameter. After spinning, the diameter of the spool was reduced so that constrained shrinkage during drying to 200 °C could be avoided. When fibers dried in this manner were heat treated in fiber bundles fragmentation did not occur and the mean strength increased to ≈ 1.7 GPa (1300 °C heat treatment). When the same fibers were individually supported in a crucible by as single Al_2O_3 rod, the mean strength value increased to 2.3 GPa with a relatively small scatter in strength values. These results show that any constraint to shrinkage (e.g., friction between fibers processed in bundles) is detrimental. Fibers are most prone to fragmentation and partial cracking during the drying step where, it is presumed, the precursor fiber has its lowest critical stress intensity factor.

Fiber strength was also determined as a function of the maximum heat treatment temperature. It was observed that the fibers were weak prior to complete pyrolysis, viz., strengths were < 0.4 GPa after heat treatments < 400 °C. After a heat treatment at 500 °C, the average strength increased to ≈ 1 GPa, and then decreased to ≈ 0.5 GPa after a heat treatment at 800 °C. This drop in strength appears to be related to the formation of a porous network due to the oxidation of residual free carbon as reflected in the densification data shown in Fig. 2, and by direct observations. As shown in Fig. 11, the average strength increases to ≈ 1 GPa after heat treatments at either 1000 or 1100 °C. The fibers become stronger during heat treatments to 1300 °C, where the maximum average value of 2.3 GPa was obtained. Comparing these strength data to the densification behavior reported in Fig. 2, it can be concluded that this strengthening is concurrent with

the fiber becoming fully dense. Since similar flaws (large voids) appeared to be common fracture origins over this temperature range, it appeared that the fully dense material had the highest critical stress intensity factor.

As shown in Fig. 11, the average strength decreased with heat treatments at 1400 and 1500 °C. This strength decrease appeared to be caused by grain growth, viz., larger grains were apparent at some fracture origins.

The result of this work showed that the strongest fibers were produced when a) the shrinkage during drying and subsequent pyrolysis was not constrained, b) the fibers were fully dense (excluding distributed voids observed at fracture origins), and c) the dense fibers had their smallest grain size. Preliminary work with a precursor producing cubic fibers (ZrO_2 + 8 m/o Y_2O_3) which undergoes extensive grain growth at 1400 °C, strongly suggests that large

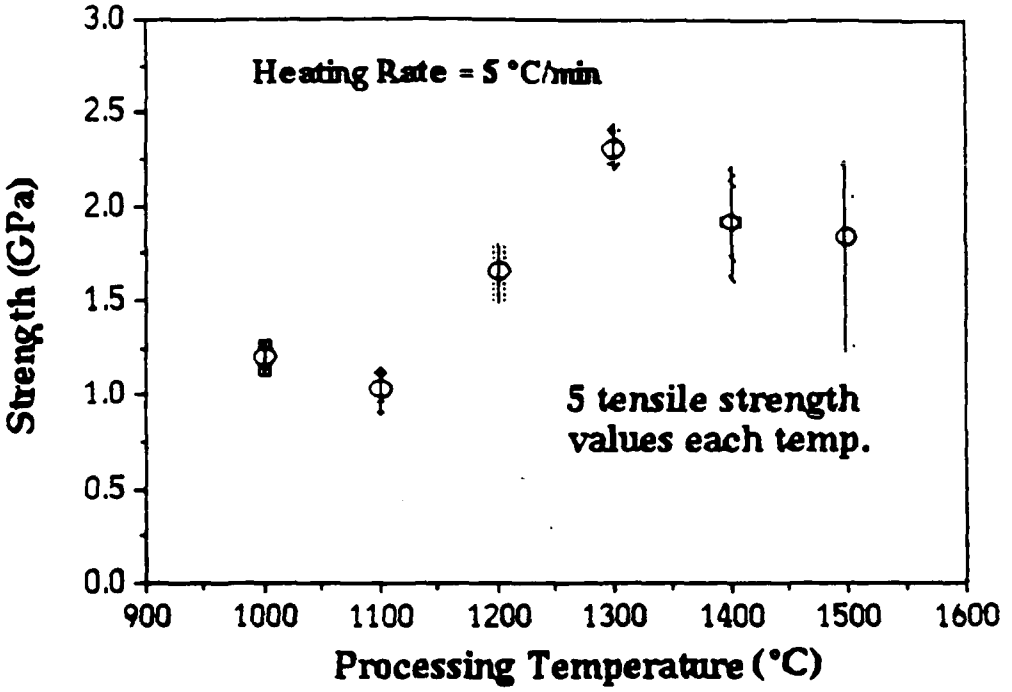

Figure 11 Average tensile strength of ZrO_2 +3 mole %Y_2O_3 fibers continuously spun from a liquid precursor vs heat treatment temperature.

grains are a critical flaw population. The current work suggests that the voids observed at fracture origins are primarily caused by air that is trapped within the liquid precursor that becomes incorporated into the fiber during spinning as a small bubble. It appears that the most probable source of this entrapped air occurs when the polymer powder is mixed with the viscous precursor. This observation suggests processing changes should be made that avoid entrapped air.

3. References

1. G. S. A. M. Theunissen, A. J. A. Winnubst, and A. J. Burggraaf, "Segregation Aspects in the ZrO_2-Y_2O_3 Ceramic Systems," J. Mater. Sci. Lett. 8 55-7 (1989).

2. S. L. Huang and I-W. Chen, "Grain Growth Control in Zirconia Polycrystals," presented at the 4th International Conference on Zirconia, Anaheim, CA, Nov. 1989.

3. F. F. Lange, D. B. Marshall, and J. R. Porter, "Controlling Microstructures Through Phase Partitioning From Metastable Precursors: the ZrO_2-Y_2O_3 System," p 519-32 in Ultrastructure Processing of Advanced Ceramics, Ed. by J. D. Mackenzie and D. R. Ulrich, John Wiley, NY (1988).

4. Summary of Technical Reports

Technical Report No. 1

TEM Studies on Phases and Phase Stabilities of Zirconia Ceramics, M. Rühle, L.T. Ma, W. Wunderlich, and A.G. Evans, Electron Structure and Phase Stability in Advanced Ceramics, Physica B 150, 86-98 (1988)

TEM studies for different ZrO_2 ceramics are reported. Observations are described to characterize the atomistic defects present in Mg-PSZ. TEM is applied to study phase stability and transformation in Y-TZP. The nucleation of stable m-ZrO_2 at stress singularities associated with grain boundaries was studied in situ and related to strains and strain distributions determined by high resolution electron microscopy.

Technical Report No. 2

Instability of Polycrystalline Thin Films: Experiment and Theory, K.T. Miller, F.F. Lange, and D.B. Marshall, J. Mater. Res. 5 [1] 151-60 (1990).

The break-up of a dense, polycrystalline thin film into isolated, individual grains is described. This break-up is shown to result from grain growth. Two mechanisms are observed to uncover the substrate: a) very small grains disappear to expose the substrate and b) large amplitude perturbations at triple points grow as grain surfaces become spherical. Calculations show that the free energy of the system continuously decreases during this uncovering process when the grain size to film thickness ratio is greater than a critical value. Calculations and experimental observations show that the film will continue to cover the substrate if the critical size to thickness ration is not exceeded. These results are important when thin films are used either to coat fibers for composite materials or for electronic devices, i.e., grain growth must be controlled.

Technical Report No. 3

Morphological Stability of Polycrystalline Fibers, K.T. Miller and F.F. Lange, Acta Met. 37 [5] 1343-7 (1989).

The effect of grain growth on the morphological stability of polycrystalline fibers, constrained by a matrix, was determined. Analogous to thin films, grain growth was observed to cause the fiber to break-up into individual grains when the grain size to fiber diameter ratio exceeded a critical value. Calculations show that the free energy of the system continuously decreases as this break-up occurs. These results are important when polycrystalline fibers are intended to reinforce a matrix to produce a stronger composite material, viz., extensive grain growth must be avoided to maintain a fiber morphology within the composite.

Technical Report No. 4

Powder Processing Science and Technology for Increased Reliability
F. F. Lange, J. Am. Ceram. Soc. 72 [1] 3-15 (1989).

The science and technology for eliminating heterogeneities from powders using the colloidal approach, consolidating colloidally prepared powders to form engineering shapes, densifing these shapes and methods of controlling microstructure are reviewed with the goal of increasing mechanical reliability through processing reliability. Research directions, required to implement these concepts, are summarized.

Technical Report No. 5

Single Crystal Zirconia Thin Films from Liquid Precursors
K. T. Miller and F. F. Lange, MRS Symp. Proc. Vol. 155, pp 191-7, Processing Science of Advanced Ceramics, Ed. by I.A. Aksay, G.L. McVay, D.R. Ulrich, MRS, Pitts. (1989).

Epitaxial, single crystal films of ZrO_2 (Y_2O_3) were formed on (100) oriented

single crystal substrates of ZrO_2 (9.5 mol% Y_2O_3) using water-based solutions of zirconium acetate and yttrium nitrate as a precursor. Film compositions of ZrO_2 (0-40 mol% Y_2O_3) were examined; since the lattice parameter of ZrO_2 (Y_2O_3) increases with yttria content, the lattice mismatch was systematically varied to a maximum of 1.5%. Precursor films were deposited by spin coating, pyrolyzed, and held for 1 hour at 900°C, 1000°C, and 1100°C. X-ray diffraction showed that a strongly oriented film had developed after pyrolysis of the precursor. In addition, all samples, except those treated at 1100°C containing 6-15 mol% Y_2O_3, gave (111) peaks, indicating film polycrystallinity. Electron back-scattering patterns showed that epitaxial single crystals were formed at 1100°C for films containing 3-20 mol% Y_2O_3. Scanning electron microscopy showed that the epitaxial films had a porous structure. These results indicate that the epitaxy is a two stage process: oriented nucleation upon pyrolysis, followed, for low mismatches, by subsequent consolidation into a single crystal film above 1000°C.

Technical Report No. 6

Grain Growth of Tetragonal Zirconia in Some Binary Systems
I. Nettleship, D. K. Leung, F. F. Lange and M. Rühle, J. Am. Ceram. Soc. (in review).

Solid solutions derived from aqueous zirconium acetate and metal nitrates have been used to study grain growth of tetragonal zirconia in binary oxide systems. The effects of substituting cations of differing valency and ion size were examined. Fine grained tetragonal zirconia was observed in all the systems of the type ZrO_2-M_2O_3 that were investigated and also in the ZrO_2-CaO system. Preliminary observations suggest most of these materials are in the cubic-tetragonal two phase region. In each case grain growth of the tetragonal phase at 1400°C was slower than for the ZrO_2-CeO_2 system.

Technical Report No. 7

Microcrack and Transformation Toughening of Zirconia-Containing Alumina, Marfred Rühle, Mat. Sci. & Eng. A105/106, 77-82 (1988).

Experimental studies on the microcrack and transformation toughening of zirconia (ZrO_2)-containing alumina are presented. The investigated ceramics contain about the same volume fractions of tetragonal and monoclinic ZrO_2 particles respectively. The microcrack parameters (microcrack length, microcrack density and microcrack opening) and the transformation behavior are determined by transmission electron microscopy studies. The microstructural results are used to explain the mechanical properties of the toughened material.

Technical Report No. 8

Metastable Crystallization, Phase Partitioning, and Grain Growth of ZrO_2-Gd_2O_3 Materials Processed from Liquid Precursors
D. K. Leung, C.-J. Chan*, M. Rühle**, and F. F. Lange, Sent to J. Am. Ceram.

Soc.

Aqueous mixtures of Zr-acetate and Gd-nitrate were used to prepare chemically homogeneous ZrO_2-Gd_2O_3 solid-solutions containing 0 to 9 mol% Gd_2O_3. The application of kinetically-limited equilibria concepts explains why a metastable tetragonal phase crystallizes subsequent to precursor pyrolysis from compositions containing <6.5 mol% Gd_2O_3 and a metastable cubic phase crystallizes from precursors with >6.5 mol% Gd_2O_3. Partitioning experiments for a composition containing 3 mol% Gd_2O_3 showed that the maximum equilibrium solid-solubility of Gd_2O_3 in tetragonal ZrO_2 is 1.0 ± 0.1 mol% and the minimum equilibrium solid-solubility in cubic ZrO_2 is 8.0 ± 0.2 mol% at 1400°C. Although phase partitioning appears to initiate during heating, complete partitioning at 1400°C required ~200 hr. Large compositional variations (≤ ± 1 mol% Gd_2O_3) were observed within tetragonal grains and from grain to grain during the first 50 h at 1400°C, whereas the composition of cubic grains produced during partitioning were relatively invariant. Experiments showed that this compositional variability was not present in material rapidly heated to 800°C, but was a result of partitioning. At 1400°C, growth of the tetragonal grains was very sluggish, increasing only to 3 μm after 500 h, whereas the number of larger cubic grains increased during this same period. The implications of these observations are related to the processing of rare-earth stabilized transformation toughened materials.

Technical Report No. 8

September 15, 1990

Metastable Crystallization, Phase Partitioning, and Grain Growth of ZrO_2 -Gd_2O_3 Materials Processed form Liquid Precursors

by

D. K. Leung, C.-J. Chan*, M. Rühle and F. F. Lange**

Materials Department
College of Engineering
University of California, Santa Barbara
Santa Barbara, CA 93106

Grant: AFOSR-87-0291

Department of the Air Force
Air Force Office of Scientific Research
Electronic and Material Sciences
Bolling Air Force Base, DC 20332-6448

* IBM, PO Box 218, Yorktown Heights, NY 10598
** Max-Planck-Institut für Metallforschung, Seestr. 92, D-7000 Stuttgart 1, FRG

Metastable Crystallization, Phase Partitioning, and Grain Growth of ZrO_2-Gd_2O_3 Materials Processed from Liquid Precursors

D. K. Leung, C.-J. Chan*, M. Rühle, and F. F. Lange**
Materials Department
College of Engineering
University of California
Santa Barbara, CA 93106

Abstract

Aqueous mixtures of Zr-acetate and Gd-nitrate were used to prepare chemically homogeneous ZrO_2-Gd_2O_3 solid-solutions containing 0 to 9 mol% Gd_2O_3. The application of kinetically-limited equilibria concepts explains why a metastable tetragonal phase crystallizes subsequent to precursor pyrolysis from compositions containing <6.5 mol% Gd_2O_3 and a metastable cubic phase crystallizes from precursors with >6.5 mol% Gd_2O_3. Partitioning experiments for a composition containing 3 mol% Gd_2O_3 showed that the maximum equilibrium solid-solubility of Gd_2O_3 in tetragonal ZrO_2 is 1.0 ± 0.1 mol% and the minimum equilibrium solid-solubility in cubic ZrO_2 is 8.0 ± 0.2 mol% at 1400°C. Although phase partitioning appears to initiate during heating, complete partitioning at 1400°C required ~200 hr. Large compositional variations (≤ ± 1 mol% Gd_2O_3) were observed within tetragonal grains and from grain to grain during the first 50 h at 1400°C, whereas the composition of cubic grains produced during partitioning were relatively invariant. Experiments showed that this compositional variability was not present in material rapidly heated to 800°C, but was a result of partitioning. At 1400°C, growth of the tetragonal grains was very sluggish, increasing only to 3 μm after 500 h, whereas the number of larger cubic grains increased during this same period. The impilcations of these observations are related to the processing of rare-earth stabilized transformation toughened materials.

* IBM, PO Box 218, Yorktown Heights, NY 10598

** Max-Planck-Institut für Metallforschung, Seestr. 92, D-7000 Stuttgart 1, FRG

1 Introduction

Binary zirconia compositions fabricated by densifying powders, derived from precursors calcined at temperatures <1000°C, are dense, polycrystalline materials that exhibit high fracture toughness and strength.[1, 2] In the well studied ZrO_2-Y_2O_3 system, materials called Y-TZP (Tetragonal Zirconia Polycrystals) with compositions containing between 2 and 3 mol% Y_2O_3 are primarily composed of submicron grains of tetragonal ZrO_2 and occasional, large (>1μm) cubic grains. All evidence suggests that the high fracture toughness of these materials is primarily due to the stress-induced tetragonal to monoclinic phase transformation that occurs ahead of a propagating crack. In other words, tetragonal grains are the toughening agent in these materials.

Because the susceptibility of the tetragonal grains to stress-induced transformation is expected to depend on composition,[3] it is of great interest to know the Y_2O_3 content of the tetragonal phase at a given processing temperature. If it is assumed that the maximum Y_2O_3 content cannot exceed the equilibrium solid-solubility limit, then equilibrium phase diagrams would be useful to define this limit. As reviewed by Yoshimura,[4] a number of investigators have attempted to determine the equilibrium solid-solubility limit of Y_2O_3 in the tetragonal phase and the boundaries of the two phase (tetragonal + cubic) region in the ZrO_2-Y_2O_3 system. However, indisputable values remain elusive. Commonly cited values include those of Scott,[5] who initially reported 2.1 and 7.6 mol% Y_2O_3 as the equilibrium composition of tetragonal and cubic structures at 1400°C and subsequently reported[6] a value of 0.5 mol% as the equilibrium solubility limit for the tetragonal phase at 1450°C. Alternatively, Rühle and Heuer[7] measured average values of 2.3 and 7.4 mol%, respectively, for commercial materials processed for short periods at 1400°C. Ruh[8] reported 1.5 mol% as the maximum solubility of Y_2O_3 in tetragonal zirconia at 1400°C.

More recently, Lange *et al.* [9] have shown that ZrO_2-Y_2O_3 materials produced from mixed liquid precursors with compositions between 1 to 3 mol% Y_2O_3 heat treated for short periods (≤ 1 h) at 1400°C are composed of only submicron tetragonal grains. Analytical electron microscopy showed that after longer heat treatment periods large cubic grains containing ~7 mol% Y_2O_3 developed. At the same time, the average Y_2O_3 content within the tetragonal grains was highly variable, differing by as much as ± 1 mol% from grain to grain, and decreased with increasing time at temperature. It was concluded that powders produced from binary precursors can result in a metastable tetragonal phase that slowly partitions over long periods (at

least up to 200h) at 1400°C to a tetragonal phase with a maximum solubility of ≤1.25 mol% Y_2O_3 and a cubic phase containing ~7 mol% Y_2O_3. Since all current Y-TZP are processed from precursor-derived powders, these results strongly suggest that the Y_2O_3 content of the tetragonal phase bear little, if any, relation to the equilibrium solid-solubility limit, but instead, depend on the time and temperature used to densify the powders.

Another characteristic common to all Y-TZP materials is their extremely small grain size and sluggish grain growth kinetics.[9, 10] Previous studies suggest that the retention of the tetragonal phase after high temperature processing depends on grain size.[1, 2] That is, the grain size must be smaller than a critical value. This sluggish grain growth phenomenon is observed for compositions containing between ~1 to 6 mol% Y_2O_3, in the approximate two phase region of the equilibrium phase diagram. More specifically, in this compositional range, the slow grain growth is observed only for the tetragonal grains, whereas cubic grains grow faster and thus become large. Outside this compositional range, the apparent single phase tetragonal and cubic materials exhibit more rapid grain growth kinetics, with an average grain size generally an order of magnitude larger relative to identically processed materials within the apparent two phase regime.[10]

Lange *et al.*[9] have shown that a material produced with a commercial powder containing 3 mol% Y_2O_3 increased its critical stress intensity factor from 3 MPa $m^{1/2}$ to 10 MPa $m^{1/2}$ after heat treatments at 1400°C for 1 and 100h, respectively. The grain growth behavior was also characterized as increasing from 0.3 μm to 0.6 μm for the same heat treatment period. Since this material did not contain monoclinic phase, which appears after heat treatments of ≥120h, but increased its cubic phase content during heat treatment, it was concluded that the increased fracture toughness resulted from the increased susceptibility of the tetragonal phase to stress-induced transformation as its Y_2O_3 content decreased during phase partitioning. It was also concluded that any relations between grain size and fracture toughness would be obscured by the apparent partitioning phenomenon.

Based on current evidence, there are many unanswered questions concerning the metastability of precursor-derived binary ZrO_2 powders, limits of solid-solubility at processing temperatures, phase partitioning during processing, sluggish grain growth of the tetragonal phase, and the relation of these phenomena to transformation toughening. In an attempt to gain a better understanding of these phenomena, a study was undertaken to detail the phase relations, partitioning

reactions, and grain growth of a ZrO_2-rare earth binary system. Since an important part of this study involved analytical electron microscopy, the ZrO_2-Gd_2O_3 binary system was chosen because the EDS spectra for Zr and Gd are readily distinguishable, whereas major EDS peaks for the Y spectrum are nearly coincident with those of Zr. Although Yoshimura[4] has shown that many ZrO_2-rare earth binary systems exhibit similar phase relations and lattice parameter changes with composition, only limited phase equilibria data exists for this system.[11, 12] With regard to the grain growth phenomenon, Nettleship *et al.*[13] have shown that grain growth in different ZrO_2-trivalent rare-earth systems, including ZrO_2-Gd_2O_3, is similar to that of Y-TZP. In addition, preliminary evidence suggested that similar compositions in the ZrO_2-Gd_2O_3 system exhibited similar partitioning kinetics relative to those in ZrO_2-Y_2O_3. Thus, the ZrO_2-Gd_2C_3 system provided an opportunity for determining, with better chemical resolution, the possible relations between powders derived from precursors and the processing of TZP materials.

2. Experimental Procedures

2.1 Precursor Materials

Materials used in this study were prepared from a chemical route using aqueous precursors. After an initial pyrolysis to determine the conversion of the precursors to oxides, assayed amounts of Gd-nitrate† were added to a Zr-acetate solution§ to prepare chemically homogeneous ZrO_2-Gd_2O_3 solid-solutions containing 0 to 9 mol% Gd_2O_3. A small amount of ethanol was added to expedite the room temperature drying of thin liquid layers held within a plastic dish. Upon drying, transparent, X-ray amorphous Zr-acetate flakes were formed. Although the flakes cracked during drying, relatively large (5mm x 5mm) pieces were readily available for different studies. These precursor flakes were used in the studies described below.

2.2 Determination of Chemical Homogeneity

As initial compositional variations in the specimen may affect the interpretation of other results, chemical fluctuations within materials formulated to contain 1.0 and 3.0 mol% Gd_2O_3 specimens were assessed to ensure that the liquid precursors yielded homogeneous materials. Direct compositional measurement of the acetate precursor with high spatial resolution was impossible because of out-gassing within the TEM vacuum. Analysis was preformed on pyrolyzed materials instead. Crushed and dried acetate powder was quickly heated ("upquenched") by

directly placing the precursor powder in a furnace at 800°C where free carbon, a residue of pyrolysis, disappeared by oxidation but solid-state diffusion was too slow to effect partitioning reactions. The subsequently produced oxide powder was suspended on a holey carbon grid for TEM/EDS investigation.[¶] The particles were agglomerates with a crystallite size of ~20 nm. The Gd_2O_3 content in ~150 nm regions were analyzed using energy dispersive spectroscopy (EDS)[¥] Quantification was based on the thin film approximation using the SMTF software program [¥]. The experimental proportionality constant (k-factor) for EDS analysis was obtained by sampling 30 regions within each synthetic standard of acetate-derived ZrO_2-10 mol% Gd_2O_3 and ZrO_2-15 mol% Gd_2O_3 single phase cubic specimens. Peak intensities of Zr-K_α and Gd-L_α were used in quantification. Because of the low Gd concentrations in many of the compositions of interest and the need for small statistical errors, counting times as long as 1000s were used to obtain a statistical error of ±0.1 mol% Gd_2O_3 for these and other studies. In addition, extreme care was taken to limit beam and specimen drift to less than 50 nm.

2.3 Crystallization of Metastable Phases *vs.* Composition

To study the formation of metastable phases, differential thermal analysis (DTA)[††] was used in combination with thermogravimetric analysis (TGA)[§§] to determine the temperature at which ZrO_2-Gd_2O_3 solid-solutions crystallized from the amorphous acetate-nitrate mixture. Precursor powders with compositions within the apparent two phase region (2 to 8 mol% Gd_2O_3 prepared in 0.5 mol% increments) were upquenched in a Pt crucible to a temperature above the DTA crystallization temperature. Experiments showed that such a rapid heating rate precluded significant amounts of partitioning, so that the crystalline phase produced after pyrolysis is maintained. Powder X-ray diffractometry[*] was used for phase determination. The cubic (400) peak and the (400) and (004) tetragonal peaks were used for phase determinations.

2.4 Phase Partitioning at 1400°C

Phase equilibria and partitioning kinetics were determined using analytical electron microscopy on specimens containing 3 mol% Gd_2O_3 that had been heat treated at 1400°C for 0 to 500h. For these studies, the precursor flakes were heated in air at a rate of 1°C/min to 800°C for 2h to both pyrolyze the precursor and remove the residual carbon by oxidation prior to heating to 1400°C. After the 1400°C heat treatment, TEM specimens were prepared by careful dimpling and ion thinning.

The composition of individual grains was measured to within ± 0.1 mol% Gd_2O_3 using a 150 nm probe. Compositions of regions within individual grains were also determined to the same precision using a 50 nm probe. Care was taken to ensure that non-overlapping grains were observed for these and other compositional measurements.

2.5 Grain Growth Studies

The same ZrO_2-3 mol% Gd_2O_3 flakes used for phase partitioning studies were also used to determine grain growth kinetics. The average grain size for different annealing times was obtained using the line-intercept method (multiplication factor = 1.5) on SEM micrographs of sintered surfaces. No difference was observed between fracture surfaces and sintered surfaces. Because the system partitions into large cubic (as confirmed by TEM) and small tetragonal grains during heat treatment, the intercepts of very large grains (>3 times the average size), were assumed to be cubic grains, and were subtracted in calculating the average grain size. All grains were counted for specimens annealed for long periods (≥ 200h) where grains of the two phases were not readily distinguishable in size. The grain size with respect to composition (0 to 9 mol% Gd_2O_3) was also determined using the same procedure for a heat treatment at 1400°C of 1 h.

3. Results

3.1 Chemical Homogeneity

As shown in Fig. 1, no significant compositional differences were found in 150 nm diameter regions in powder specimens upquenched to 800°C and held for 6 min. It can be concluded that liquid precursors can yield very homogeneous starting materials. Since the 150 nm probe used to analyze the agglomerated particles is approximately half the grain size for materials heated for short periods at 1400°C, it must be concluded that compositional differences reported below are due to partitioning and not caused by compositional variations in the precursor.

3.2 Metastable Phases vs Composition

Results from thermogravimetric analysis performed with a heating rate of 5°C/min showed that major weight loss during pyrolysis of the dried, Gd containing Zr-acetate precursor occurs at ~350°C, although complete removal of residual carbon does not occur until 800°C with a corresponding weight loss. A strong DTA exotherm was observed at ~450°C. Since this exotherm did not correspond to a

weight loss, it was assumed that it resulted from the crystallization of the amorphous, pyrolyzed precursor. This is in agreement with previous data for Zr-acetate containing Y-nitrate.[14, 15] In addition, precursor particles heated to 300°C were observed to be amorphous in the TEM. Beam heating caused these particles to transform to polycrystalline agglomerates with a primary crystallite size of ~5 to 10nm.

Initially, upquenching experiments were conducted at 800°C. However, the small grain size (< 50nm) in powder upquenched to <1200°C caused significant XRD peak broadening, making it difficult to determine whether the material was cubic or tetragonal for compositions close to the transition (T_o) composition. This problem was avoided by upquenching to 1200°C, where grains were large enough (~100 nm) for XRD, but still small enough to avoid spontaneous transformation to the monoclinic structure during cooling. Because heating rates are finite even during upquenching, the material was assumed to crystallize at ~450°C, despite being rapidly exposed to higher temperatures.

To confirm that partitioning was minimized during upquenching, XRD was used to observe the phases produced by slow heating and upquenching. Figure 2 illustrates the comparative XRD patterns (70°-78° 2θ) for a 5 mol% Gd_2O_3 precursor upquenched and slowly heated at 1°C/min to 1200°C. As illustrated, only the $(400)_t$ and $(004)_t$ diffraction peaks are observed for the upquenched specimen, whereas a diffuse $(400)_c$ peak is also observed for the slowly heated specimen. In addition, quantitative EDS with a 150nm probe was performed on agglomerate particles produced from a 3 mol% Gd_2O_3 precursor heated at 1°C/min to 1200°C. Figure 3 shows that the compositional scatter for these particles is much larger relative to that obtained from the same precursor upquenched to 800°C. These data clearly show that partitioning can initiate as the precursor is slowly heated to higher temperatures.

For compositions containing increasing Gd_2O_3 additions, only the tetragonal structure was observed by XRD when the material was upquenched and had a Gd_2O_3 content ≤ 5 mol%. The $(400)_t$ and $(004)_t$ diffraction peaks merged together and nearly became indistinguishable at slightly higher Gd_2O_3 contents. The cubic structure was clearly indicated by the presence of a sharp $(400)_c$ diffraction peak for compositions containing ≥7.5 mol% Gd_2O_3. For materials containing 6-7 mol% Gd_2O_3, it was impossible to distinguish the two structures. Thus, the T_o (transition) composition for the crystallization temperature of 450°C was estimated to be 6.5 ± 0.5 mol% Gd_2O_3. The lattice parameters of metastable tetragonal and cubic ZrO_2-Gd_2O_3

solid-solutions upquenched to 1200°C for 6 min are given in Fig. 4. A silicon internal standard was used to correct for systematic errors in the diffractometer. The change in lattice parameters with respect to composition in ZrO_2-Gd_2O_3 is very similar to that of other ZrO_2-trivalent rare-earth oxide binaries as reported by Yoshimura.[4]

The metastable nature of the tetragonal phase was confirmed by the partitioning experiments described below. Cubic metastability was confirmed by upquenching a ZrO_2-7.5 mol% Gd_2O_3 powder to 1400°C and holding for 10 hours. As shown in Fig. 5, the $(400)_c$ peak shifted to a lower 2θ position after heating, with the simultaneous appearance of a $(400)_t$ peak, which clearly demonstrates partitioning of the as-upquenched material.

3.3 Phase Partitioning

Partitioning of metastable tetragonal material containing 3 mol% Gd_2O_3 to its equilibrium cubic and tetragonal phases at 1400°C is shown in Fig. 6. Each data point reports the composition of an individual grain. The error bars represent uncertainty due to counting statistics. The number of grains analyzed in Fig. 6 is not representative of the volume fraction of each phase. Cubic grains were rarely found in specimens heat treated for short times ($\leq$ 5 h). When they were observed, they were much larger (>3 times) relative to the smaller tetragonal grains. For heat treatment periods $\leq$ 5 h, the tetragonal grains did not transform during either specimen preparation or observation, but for periods $\geq$ 10 h they were either easily transformed to the monoclinic structure by beam heating in the TEM or transformed prior to observation.

Figure 6 shows that the average Gd_2O_3 content of the tetragonal grains decreases with increasing heat treatment. The composition of cubic grains, on the other hand, remained at 8.0 $\pm$ 0.2 mol% Gd_2O_3 while their apparent size and volume fraction increased during partitioning. The composition within each observed cubic grain was very uniform. On the other hand, the compositional differences within tetragonal grains and from grain to grain was highly variable, up to ~$\pm$1 mol% for heat treatment periods of $\leq$ 5h for both cases.

The apparent equilibrium solubility of Gd_2O_3 in the tetragonal structure was found by allowing partitioning to progress until compositional variations from grain to grain and within single grains were equal to the counting statistics determined precision of $\pm$ 0.1 mol% Gd_2O_3. With this criterion, equilibrium was achieved after 200h at 1400°C. The maximum solid-solubility of Gd_2O_3 in tetragonal

zirconia at 1400°C is therefore 1.0 ± 0.1 mol%. Thus, the equilibrium compositions of the tetragonal and cubic phases at 1400°C are 1.0 ± 0.1 and 8.0 ± 0.2 mol% Gd_2O_3, respectively. With these phase boundaries, the 1400°C equilibrium microstructure of the ZrO_2-3 mol% Gd_2O_3 material contains ~30 vol% cubic grains as determined by the lever rule.

Figure 7 shows that during initial stages of partitioning (5h at 1400°C) appreciable compositional variations can exist within a single tetragonal grain. Grain to grain variations can still be observed after 50h as shown in Fig. 8. No evidence to suggest that cubic precipitates might exist within the tetragonal grains to account for the observed compositional variability was obtained. Silica and alumina rich intergranular phases, presumably introduced from the alumina setter tile during heat treatment, were found in a limited number of regions. However, no differences in the relative grain size and composition were observed when compared with specimens wrapped in Pt foil prior to heat treatment to prevent silica and alumina contamination.

3.4 Grain Growth at 1400°C

The SEM microstructure of ZrO_2-3 mol% Gd_2O_3 heat treated at 1400°C for 5, 50, and 500 hours is shown in Fig. 9. Tetragonal grain size as a function of heat treatment time is plotted in Fig. 10. The material heat treated at 1400°C for 1 minute has an average grain size of 0.45 μm. Even after 500 hours the tetragonal grains have grown only to ≈ 3 μm.

Figure 11 illustrates the grain size of the tetragonal phase versus composition for specimens heated to 1400°C for 1h. These results clearly show that although none of these materials are fully partitioned, the size of the tetragonal grains is nearly constant within a large fraction of the apparent two phase field (*i.e.* between 1 and 8 mol% Gd_2O_3). These data also show that the average size of the tetragonal grains decrease as their composition approaches the equilibrium solid-solubility limit of 1 mol% Gd_2O_3.

4 Discussion

4.1 Use of Kinetically Limited Phase Equilibria to Predict Metastable Crystal Structures

For TZP compositions processed within the two phase region, equilibrium dictates the co-existence of stabilizer-poor tetragonal and stabilizer-rich cubic phases.

But, as illustrated here, only one structure is observed to crystallize during and subsequent to the pyrolysis of the ceramic precursor. The crystallization of only one phase in a two phase region can be explained with *kinetically-limited* phase equilibria concepts.[16] These concepts were developed to explain and predict the metastable phases formed during rapid solidification of metal alloys, but apparently have not been used previously to predict the crystallization subsequent to the pyrolysis of ceramic precursors.

The use of kinetically-limited concepts implies that the system undergoes a phase change which can yield more than one phase and either a melt or a glass is crystallized at a temperature where diffusion is very limited. In the present case, crystallization occurs at very low temperatures during and/or subsequent to precursor pyrolysis. Figure 12 illustates the hypothetical free energy vs compositions functions for the tetragonal and cubic structures at a temperature where the precursor crystallizes. A precursor with a formulated composition C_f is used to illustrate the use of kinetically-limited phase equilibria. At equilibrium, tetragonal and cubic with compositions C_t and C_c should co-exist, in amounts given by the lever rule. However, under conditions of limited diffusion, the glassy, pyrolyzed precursor will reduce its free energy (ΔG_{cry}) by crystallizing to a structure with the lowest free energy. T_o is defined as the composition where both metastable tetragonal and cubic structures have the same free energy at a given temperature. The locus of T_o composition with respect to temperature yields a T_o curve in temperature vs composition space. The T_o curve lies within the two phase region defined by the C_t and C_c curves, i.e., the boundaries of this two phase field in temperature vs composition space. Compositions to the left of T_o ($C_f < T_o$) will crystallize with a tetragonal structure and those to the right ($C_f > T_o$) will crystallize with a cubic structure. For materials within the two phase field, *i.e.* between C_t and C_c, neither structure is in true equilibrium, but will partition to two new phases, a tetragonal phase with composition C_t and a cubic phase with composition C_c, if the temperature is such that long range diffusion is not limited. Based on the data presented above, the T_o composition for this portion of the ZrO_2-Gd_2O_3 binary system is estimated to be 6.5 ± 0.5 mol% Gd_2O_3 at the apparent crystallization temperature of ~450°C.

4.2 Phase Partitioning in Gd-TZP

From Figs. 3 and 6 it appears that partitioning of the cubic phase in Gd-TZP can initiate during heating and continues at the processing temperature, taking

~200h at 1400°C to reach equilibrium. For compositions containing <6.5 mol% Gd_2O_3, cubic grains with a size less than that of the metastable tetragonal grains (<10 nm), would be expected to preferentially precipitate at low interfacial energy sites, such as 2-, 3- and 4-grain junctions, during the early stages of partitioning. Since the metastable tetragonal grains grow very quickly during heating, increasing in size from ~20 nm at 800°C to ~450 nm at 1400°C, these small cubic precipitates may be engulfed by rapidly growing tetragonal grains. Although discrete cubic precipitates were not observed within tetragonal grains in the present study, their presence could account for the large compositional variations observed within the metastable tetragonal grains. Compositional gradients are also expected as Gd, Zr, and O counter diffuse to establish an equilibrium phase assemblage.

The growth of large cubic grains within the fine-grained, metastable tetragonal matrix suggests that either very few nuclei were present during partitioning or that smaller cubic grains or precipitates produced during initial heating disappear *via* a coarsening process. How the cubic phase nucleates and grows in TZP materials is still unclear and requires further investigation. Such an understanding may provide insight into controlling the size and distribution of cubic grains within the microstructure.

As illustrated in Fig. 12, the absolute value of the free energy change per unit volume driving partitioning (ΔG_p^o) decreases as the overall composition approaches one of the two equilibrium compositions, *i.e.*, $\Delta G_p^o \rightarrow 0$ when $C_f \rightarrow C_t$ or C_c and $\Delta G_p^o < 0$ when $C_t < C_f < C_c$. It might be reasoned that the very sluggish phase partitioning observed here are caused by low Gd and Zr diffusivities. On the other hand, large compositional gradients are observed within partitioning grains. Because the lattice parameters of the metastable tetragonal material strongly depends on composition, as shown in Fig. 4, compositional gradients will produce strain gradients and therefore strain energy within the partitioning tetragonal grains. It can thus be suggested that if the strain energy per unit volume, ΔU_{se}, is comparable in magnitude to ΔG_p^o, it will lower the driving potential, and possibly the rate of partitioning.

4.3 Grain Growth in TZP

The average size of tetragonal grains in material initially containing 3 mol% Gd_2O_3 increases rapidly from ~10 nm after pyrolysis to 450 nm in the 2 h needed to reach 1400°C. However, at 1400°C grain growth is extremely sluggish relative to other oxides. Three explanations for the anomalous grain growth behavior in TZP

have been proposed. First, Theunissen *et al.*[17] proposed a solute-drag model based on an apparent equilibrium segregation of yttria to grain boundaries. Second, a space-charge drag model based on the segregation of aliovalent additives has been advanced by Huang and Chen.[18] And third, based on the large differences in Y_2O_3 content from grain to grain during sluggish partitioning, Lange *et al.*[9] have suggested that coherency strains arise when boundaries between grains with different compositions move, suggesting one possible correlation between sluggish phase partitioning and slow grain growth.

Phase partitioning requires a long time, taking up to ~200h for equilibrium. This process is initially relatively fast, however, with the average Gd_2O_3 content in the tetragonal grains decreasing from 3 to 1.5 mol% within 10h. Tetragonal grain growth at the processing temperature of 1400°C is apparently very slow, as shown in Fig. 10, with the average grain size not exceeding 3μm even after 500h. It appears that slow tetragonal grain growth continues even after phase partitioning is completed. The grain size increased more during the first 200h of heat treatment, when partitioning is active, than during last 300h, when partitioning is finished. Furthermore, with the maximum solubility of Gd_2O_3 in zirconia being 1.0 mol%, it can be seen in Fig. 11 that the tetragonal grain size is decreased by Gd_2O_3 addition even before entering the two phase region.

Grain growth appears to be most suppressed when >1.5 mol% Gd_2O_3 is added. Since a fully partitioned ZrO_2-3 mol% Gd_2O_3 specimen contains ~30 vol % cubic grains and the criterion for percolation in 3 dimensions is 16 vol%,[19] the cubic phase is an interpenetrating network. It is possible that such an interconnected phase may hinder the grain growth of both phases. To test this concept, the average grain size of ZrO_2-1.5 mol% Gd_2O_3 specimens were measured. This material is expected to contain only ~7 vol % of cubic grains, as determined by the lever rule, once partitioning is fully complete. As shown in Fig. 10, no significant differences were observed between the two materials, suggesting that the equilibrium volume fraction of cubic grains plays no significant role in the sluggish growth of the tetragonal grains.

Although it is obvious that the volume fraction of the tetragonal phase must diminish as cubic grains partition and grow, current experiments show no apparent relation between grain growth and phase partitioning as suggested by Lange *et al.*[9]. While the solute-drag models proposed by Theunissen *et al.*[17] and Huang and Chen[18] could account for slow tetragonal grain growth, it is not apparent why this phenomenon would be most pronounced in the two phase region. The relevance

of solute drag models must also be questioned when an amorphous phase resides between the grains. Amorphous grain boundary phases, presumably liquid at the processing temperatures, are observed in almost all TZP materials,[20] as well as materials used in the present experiments. Experiments have shown that the tetragonal grains still exhibit sluggish grain growth despite the amorphous phase.[21] Thus, a consistent explanation of the grain growth behavior in TZP materials remains elusive.

4.4 Relation of Metastable Phase Equilibria to Processing and Properties

The current results for the ZrO_2-Gd_2O_3 system are nearly identical to the previous results [9] obtained for the ZrO_2-Y_2O_3 system. Regardless of its effect on grain growth, phase partitioning remains an important consideration in processing TZP materials. Both grain size and composition are factors which determine the susceptibility of the tetragonal phase to stress-induced transformation, and therefore, the fracture toughness of the material. Since both phenomena occur simultaneously during heat treatment, it would be difficult to separate the effect of one from the other. As discussed above, chemically derived TZP powders have tetragonal structures with a metastable composition. The rare-earth content within the tetragonal grains will decrease by partitioning with increasing heat treatment time and temperature. Observed grain to grain compositional variations will not only make some grains more susceptibility to stress-induced transformation, relative to others, but will also effect autocatalytic transformation phenomena [20], i.e., the effect of one transformed grain on the transformation of neighboring grains. Observed compositional variation within single grains will also affect the size of the nucleus needed to initiate a stress-induced transformation. Namely, rare-earth depleted regions within single grains can be considered as nuclei for this transformation. Thus, it must be recognized that the fracture toughness of TZP materials will strongly depend on the temperature and time used to densify precursor derived powders.

Acknowledgement

This work was supported by the Air Force Office of Scientific Research, under Contract No. AFOSR-87-0291.

References

1. T. K. Gupta, F. F. Lange and J. H. Bectold, "Effect of Stress Induced Phase Transformation on the Properties of Polycrystalline Zirconia Containing Tetragonal Phase," *J. Mat. Sci.* **13**, 1464 (1978)

2. F. F. Lange, "Transformation Toughening, Part 3 Experimental observations in the ZrO_2-Y_2O_3 system," *J. Mater. Sci.*, **17** 240-246 (1982).

3. C. A. Andersson, J. Greggi Jr., and T. K. Gupta, "Diffusionless Transfromations in Zirconia Alloys," pp 78-85, in Advances in Ceramics vol. 12, Science and Technology of Zirconia II. Edited by N. Claussen, M. Rühle, and A. H. Heuer, American Ceramics Society, Columbus, OH 1984.

4.. M. Yoshimura, "Phase Stability of Zirconia," *Am. Ceram. Soc. Bull.*, **67** [12] 1950-5 (1988).

5. H. G. Scott, "Phase Relationships in the Zirconia-Yttria System," *J. Mater. Sci.*, **10** 1527-35 (1975).

6. H. G. Scott, "Phase Relationships in the Magnesia-Yttria Zirconia System," *J. Aust. Ceram. Soc.*, **17** [1] 16-20 (1981).

7. A. H. Heuer and M. Rühle, "Phase Transformations in ZrO_2-Containing Ceramics: I, The Instability of c-ZrO_2 and the Resulting Diffusion-Controlled Reactions," pp. 1-13 in Advances in Ceramics vol. 12, Science and Technology of Zirconia II. Edited by N. Claussen, M. Rühle, and A. H. Heuer, American Ceramics Society, Columbus, OH 1984.

8. R. Ruh, K. S. Mazdiyasni, P. G. Valentine, and H. O. Bielstein, "Phase Relations in the System ZrO_2-Y_2O_3 at Low Y_2O_3 Contents," *J. Am. Ceram. Soc.*, **67** [9] C-190-C-192 (1984).

9 F. F. Lange, D. B. Marshall, and J. R. Porter, "Controlling Microstructures Through Phase Partitioning From Metastable Precursors: The ZrO_2-Y_2O_3 System," p. 519-32 in

Ultrastructure Processing of Advanced Ceramics. Edited by J. D. Mackenzie and D. R. Ulrich, John Wiley and Son, N.Y. (1988).

10. F. F. Lange, "Transformation Toughened ZrO_2: Correlations Between Grain Size Control and Composition in the ZrO_2-Y_2O_3 System," *J. Am. Ceram. Soc.*, **69** [3] 240-2 (1986).

11. A. Rouanet and M. Foex, C. R. *Acad. Sci., Ser. C*, **267** [15] 875 (1968).

12. A. Rouanet, Rev. *Int. Hautes Temp. Refract.*, **8** [2] 161 (1971).

13. I. Nettleship, D. K. Leung, F. F. Lange, and M.Rühle, "Grain Growth of Tetragonal Zirconia," submitted to *J. Am. Ceram. Soc.*

14. E. Leroy, C. Robin-Brosse, and J.P. Torre, "Fabrication of Zirconia Fibers from Sol-Gels," in Ultrastructure Processing of Ceramics, Glasses, and Composites, Ed. by L. L. Hench and D. R. Ulrich, pp. 219-31, John Wiley (1984).

15. M Khavari, "Strength-Processing Relation of Continuous Zirconia Fibers," M.S. Thesis, University of California, Santa Barbara, March, 1990.

16. J. C. Baker and J. W. Cahn, "Thermodynamics of Solidification," Solidification, Proc. ASM Conf., Ed. by T. J. Hughel and G. F. Bolling, Chapter 2, pp. 23-58, Am. Soc. for Metals, Metals Park, Ohio, 1971.

17. G. S. A. M. Theunissen, A. J. A. Winnubst, and A. J. Burggraaf, " Segregation Aspects in the ZrO_2-Y_2O_3 Ceramic System," *J. Mater. Sci. Lett.*, **8** 55-7 (1989).

18. S. L. Huang and I-W. Chen, "Grain Growth Control in Zirconia Polycrystals," presented at the 4th International Conference on Zirconia, Anaheim, CA, November 1989.

19. H. Scher and R. Zallen, "Critcal Density in Percolation Processes," *J. Chem. Phys.*, **53**, 3759 (1970).

20. M. Rühle, N. Claussen, and A. H. Heuer, "Microstructural Studies of Y_2O_3 Containing Tetragonal Zirconia Polycrystals (Y-TZP)"; p. 352-70 in Advances in Ceramics vol. 12, Science and Technology of Zirconia II. Edited by N. Claussen, M. Rühle, and A. H. Heuer, American Ceramics Society, Columbus, OH 1984.

21. F. F. Lange, H. Shubert, N. Claussen, and M. Ruhle, "Effects of Attrition Milling and Post-Sintering Heat Treatment on Fabrication, Microstructure and Properties of Transformation Toughened ZrO_2," *J. Mater. Sci.* **21**, 768-74 (1986).

Figure Captions

Figure 1 Gd_2O_3 content of different 150 nm regions in precursor powder specimens upquenched to 800 °C and held for 6 min. for compositions formulated with aqueous Zr-acetate + Gd-nitate solutions containing either 1 or 3 mole % Gd_2O_3. Statistical errors due to counting are represented by error bars.

Figure 2 X-ray diffraction patterns for a 5 mol% Gd_2O_3 precursor upquenched and slowly heated at 1°C/min to 1200°C showing the development of a cubic (400) peak between the tetragonal (400) and (004) peaks for the slowly heated precursor.

Figure 3 Gd_2O_3 content of different 150 nm regions in precursor powder specimens upquenched to 800 °C and heated to 1200 °C at 1 °C/min. for a composition containing 3 mole % Gd_2O_3.

Figure 4 Lattice parameters of metastable tetragonal and cubic ZrO_2-Gd_2O_3 solid-solutions upquenched to 1200°C for 6 min. A silicon internal standard was used to correct for systematic errors.

Figure 5 X-ray diffraction patterns for a 7.5 mol% Gd_2O_3 precursor upquenched to 1400°C showing showing the development of a tetragonal (400) peak after a heat treatment period of 10 h at this temperature.

Figure 6. Gd_2O_3 content of different grains (150 nm probe) for a ZrO_2-3 mol% Gd_2O_3 material heated to 1400°C and held for different periods. Larger cubic grains contained 8.0 ± 0.2 mol% Gd_2O_3, whereas Gd_2O_3 content in smaller tetragonal grains decreased to 1.0 ± 0.1 mol % after 200h. Statistical errors due to counting are represented by error bars.

Figure 7. Typical variation of Gd_2O_3 content (± 0.1 mol % Gd_2O_3, 50 nm probe) within a single tetragonal grain for a ZrO_2-3 mol% Gd_2O_3 material heated to 1400°C for 5h. A large cubic grain (7.9 mol % Gd_2O_3) is an adjacent grain, other grains are tetragonal. Small glassy pockets are observed at triple junctions.

Figure 8. Typical variation of Gd_2O_3 content (± 0.1 mol % Gd_2O_3, 150 nm probe) from grain to grain for a ZrO_2-3 mol% Gd_2O_3 material heated at 1400°C for 50 h.

Grains have transformed to monoclinic structure prior to observation. Also note large glassy pockets between some grains.

Figure 9. SEM micrographs of ZrO_2-3 mol% Gd_2O_3 material heat treated for 5, 50, and 500h at 1400 °C. Note increasing evidence of larger grains assumed to be cubic. Bands in some grains at 500 h appear to be caused by twinning during transformation.

Figure 10. Average grain size of ZrO_2- 1.5 and 3 mol% Gd_2O_3 heat treated at 1400°C vs time.

Figure 11. Average grain size of ZrO_2 with increasing Gd_2O_3 content heat treated at 1400°C for 1h.

Figure 12. Schematic of free energy vs. composition for the tetragonal, cubic and disordered (glassy) phases at the temperature where the disordered phase, with composition C_f, crystallizes during precursor pyrolysis. C_t and C_c are the equilibrium compositions of the tetragonal and cubic structures, respectively, and T_o is the composition where the free energy of both tetragonal and cubic structures are identical.

---

† Aldrich Chemical Co. Inc., Milwaukee, WI.
§ Magnesium Elektron Inc., Flemington, NJ.
¶ JEOL JSM-2000FX, Peabody, MA.
¥ Tracor-Northern 5400, Middleton, WI.
¥ Tracor-Northern 5400, Middleton, WI.
†† DuPont Differential Scanning Calorimeter 910, Wilmington, DE.
§§ DuPont Thermogravimetric Analyzer 951, Wilmington, DE.
* Scintag XDS 2000, Santa Clara, CA.

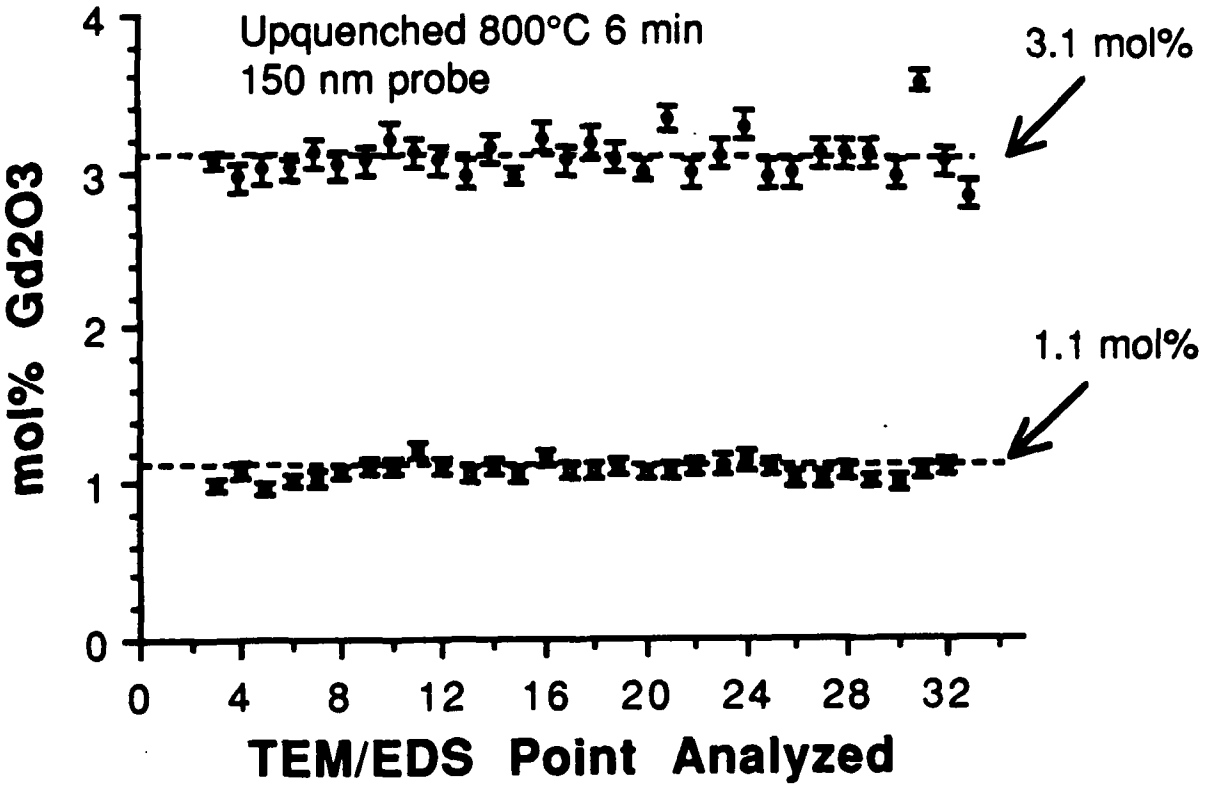

Figure 1 Gd_2O_3 content of different 150 nm regions in precursor powder specimens upquenched to 800 °C and held for 6 min. for compositions formulated with aqueous Zr-acetate + Gd-nitate solutions containing either 1 or 3 mole % Gd_2O_3. Statistical errors due to counting are represented by error bars.

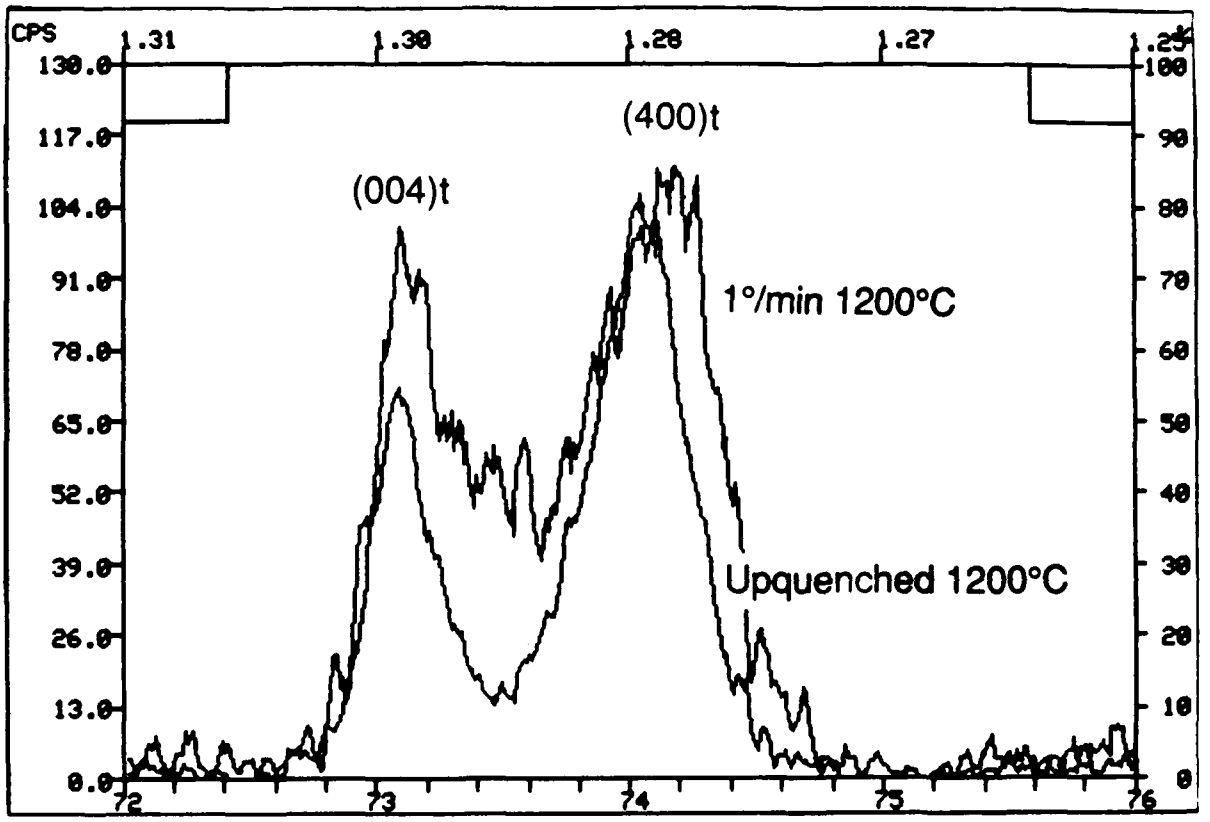

Figure 2 X-ray diffraction patterns for a 5 mol% Gd_2O_3 precursor upquenched and slowly heated at 1°C/min to 1200°C showing the development of a cubic (400) peak between the tetragonal (400) and (004) peaks for the slowly heated precursor.

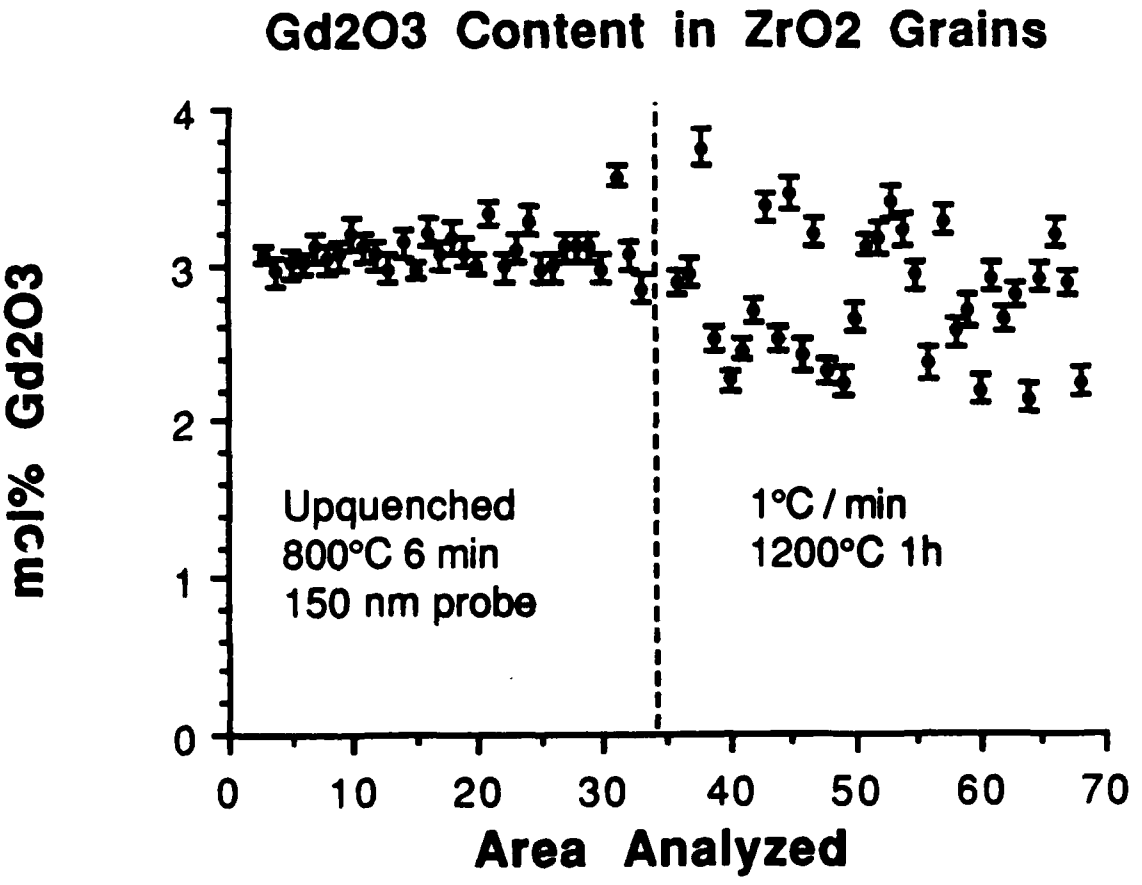

Figure 3 Gd_2O_3 content of different 150 nm regions in precursor powder specimens upquenched to 800 °C and heated to 1200 °C at 1 °C/min. for a composition containing 3 mole % Gd_2O_3.

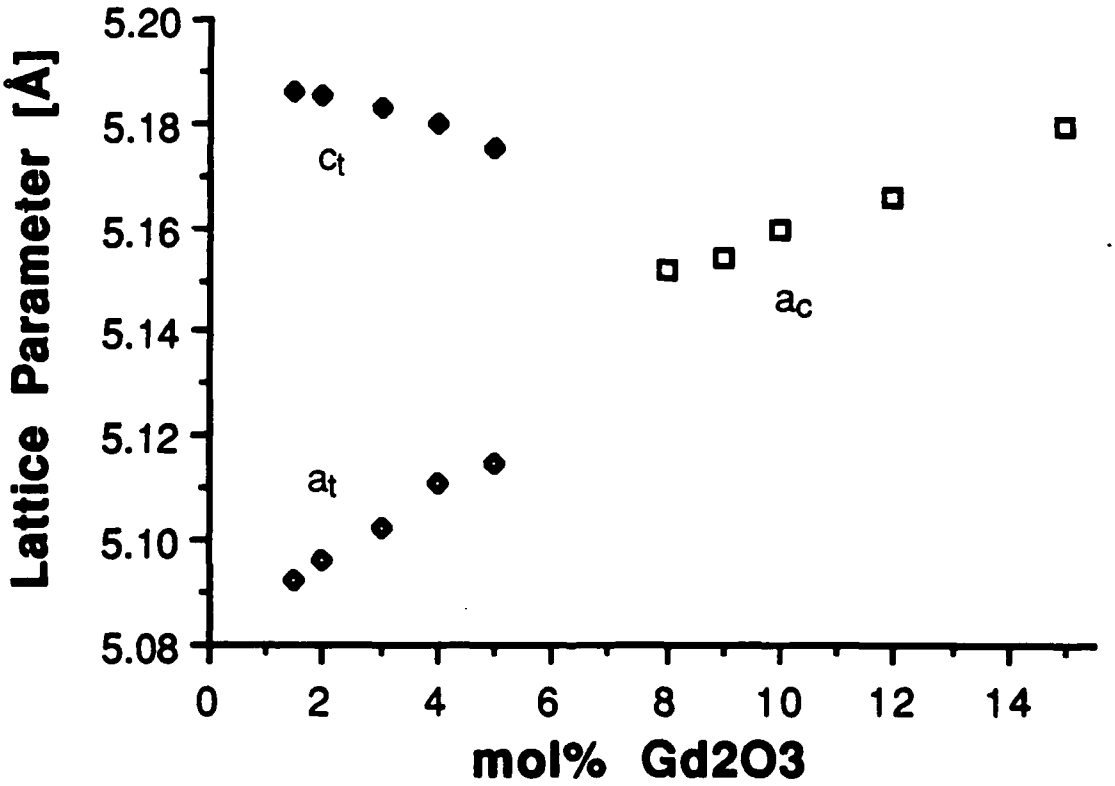

Figure 4 Lattice parameters of metastable tetragonal and cubic ZrO_2-Gd_2O_3 solid-solutions upquenched to 1200°C for 6 min. A silicon internal standard was used to correct for systematic errors.

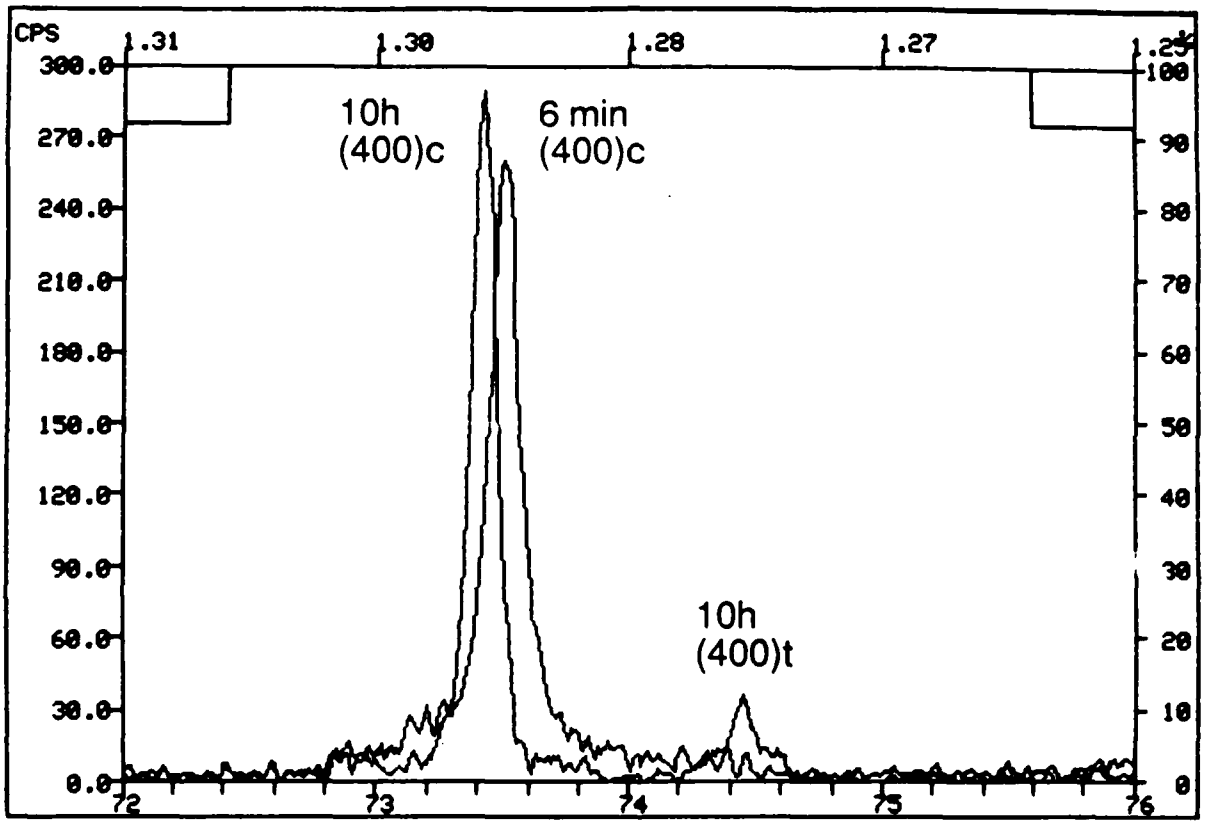

Figure 5 X-ray diffraction patterns for a 7.5 mol% Gd_2O_3 precursor upquenched to 1400°C showing showing the development of a tetragonal (400) peak after a heat treatment period of 10 h at this temperature.

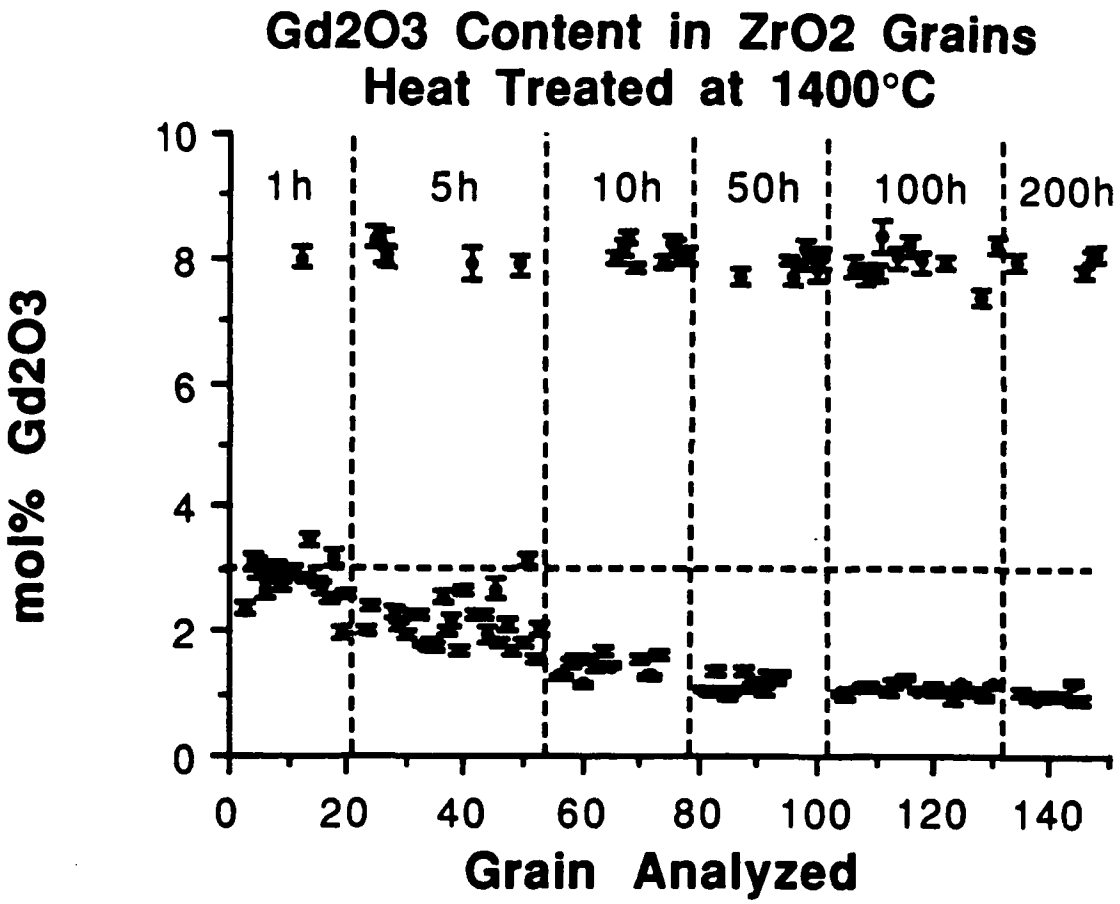

Figure 6. Gd_2O_3 content of different grains (150 nm probe) for a ZrO_2-3 mol% Gd_2O_3 material heated to 1400°C and held for different periods. Larger cubic grains contained 8.0 ± 0.2 mol% Gd_2O_3, whereas Gd_2O_3 content in smaller tetragonal grains decreased to 1.0 ± 0.1 mol % after 200h. Statistical errors due to counting are represented by error bars.

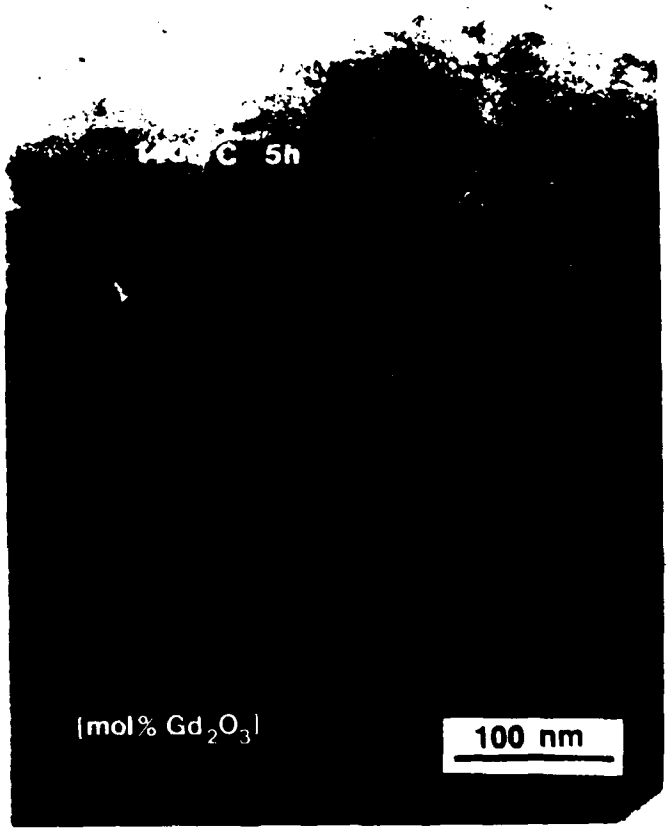

Figure 7. Typical variation of Gd_2O_3 content (± 0.1 mol % Gd_2O_3, 50 nm probe) within a single tetragonal grain for a ZrO_2-3 mol% Gd_2O_3 material heated to 1400°C for 5h. A large cubic grain (7.9 mol % Gd_2O_3) is an adjacent grain, other grains are tetragonal. Small glassy pockets are observed at triple junctions.

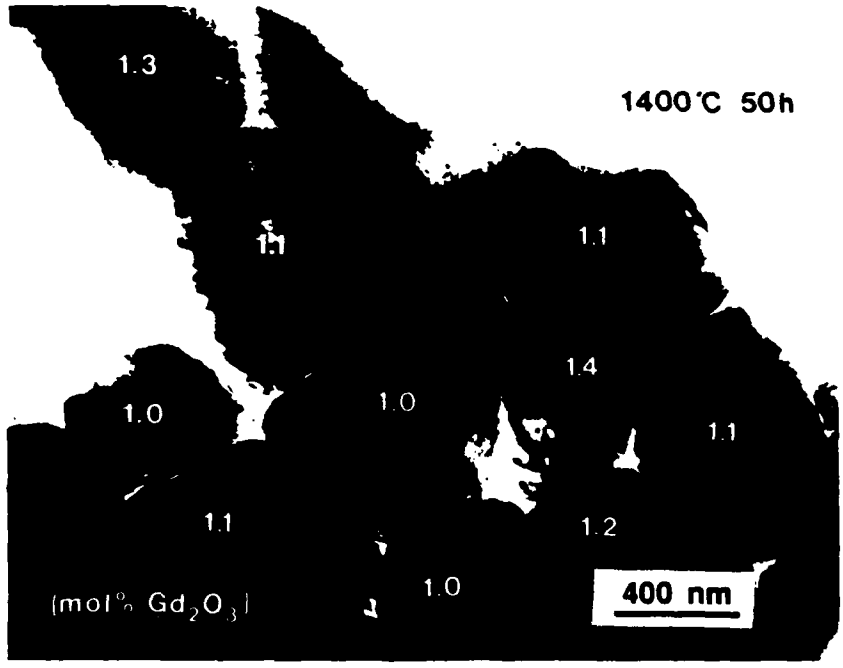

Figure 8. Typical variation of Gd_2O_3 content (± 0.1 mol % Gd_2O_3, 150 nm probe) from grain to grain for a ZrO_2-3 mol% Gd_2O_3 material heated at 1400°C for 50 h. Grains have transformed to monoclinic structure prior to observation. Also note large glassy pockets between some grains.

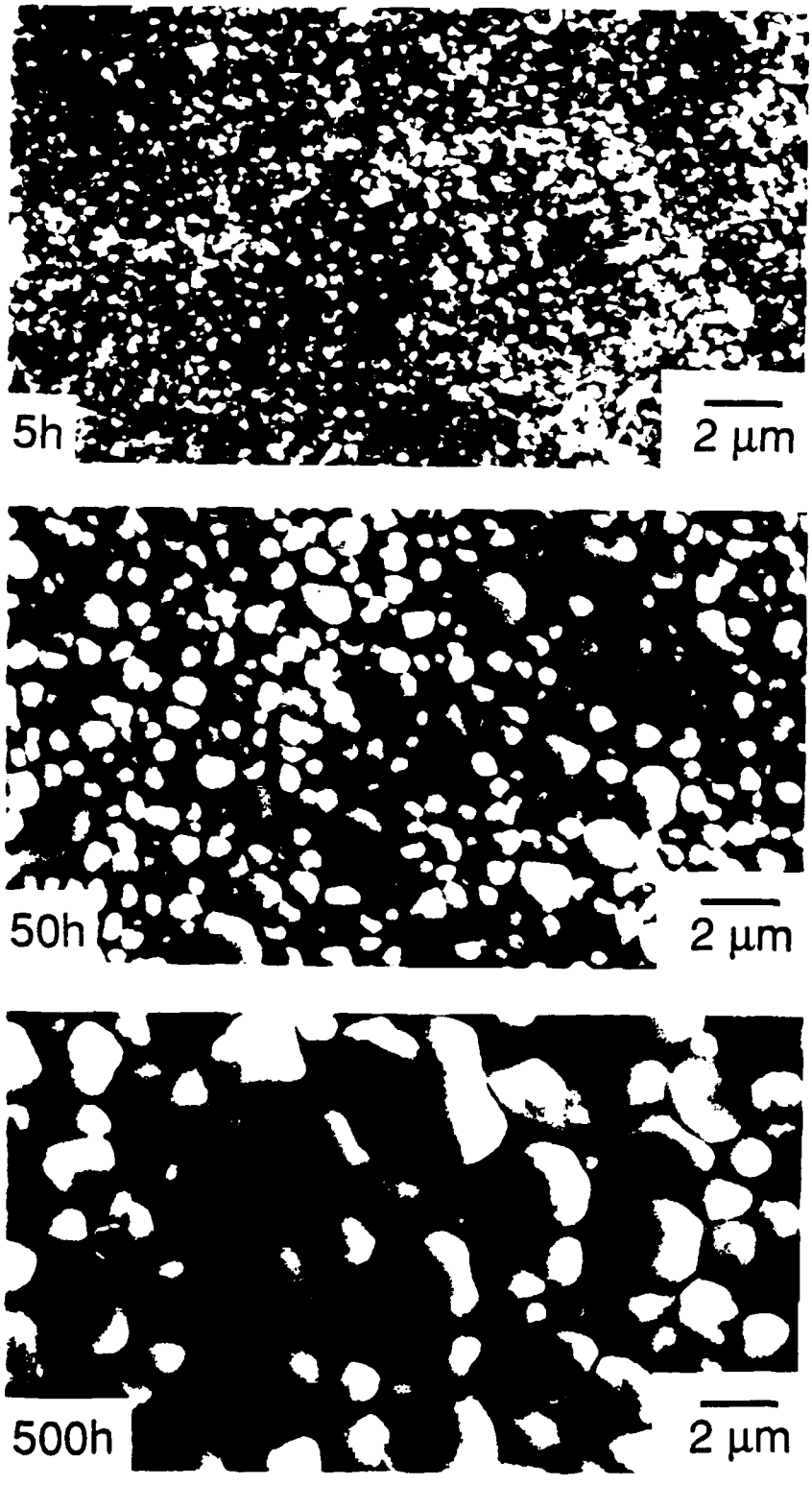

Figure 9. SEM micrographs of ZrO_2-3 mol% Gd_2O_3 material heat treated for 5, 50, and 500h at 1400 °C. Note increasing evidence of larger grains assumed to be cubic. Bands in some grains at 500 h appear to be caused by twinning during transformation.

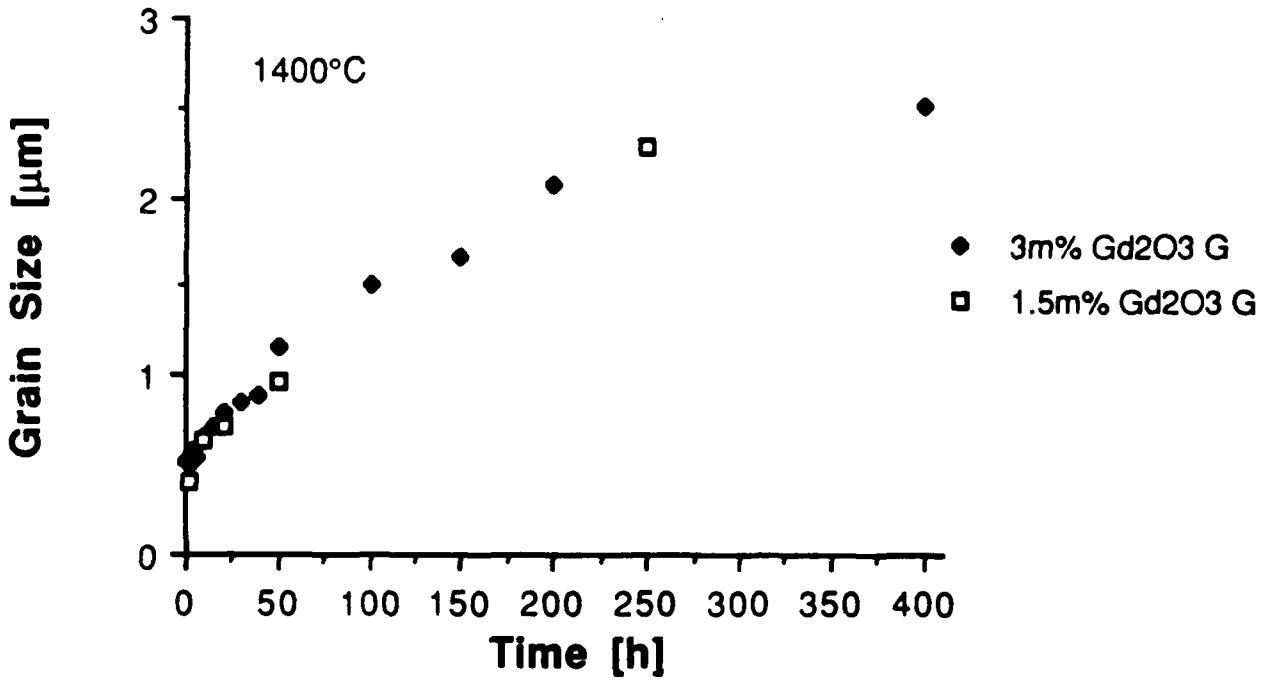

Figure 10. Average grain size of ZrO_2- 1.5 and 3 mol% Gd_2O_3 heat treated at 1400°C vs time.

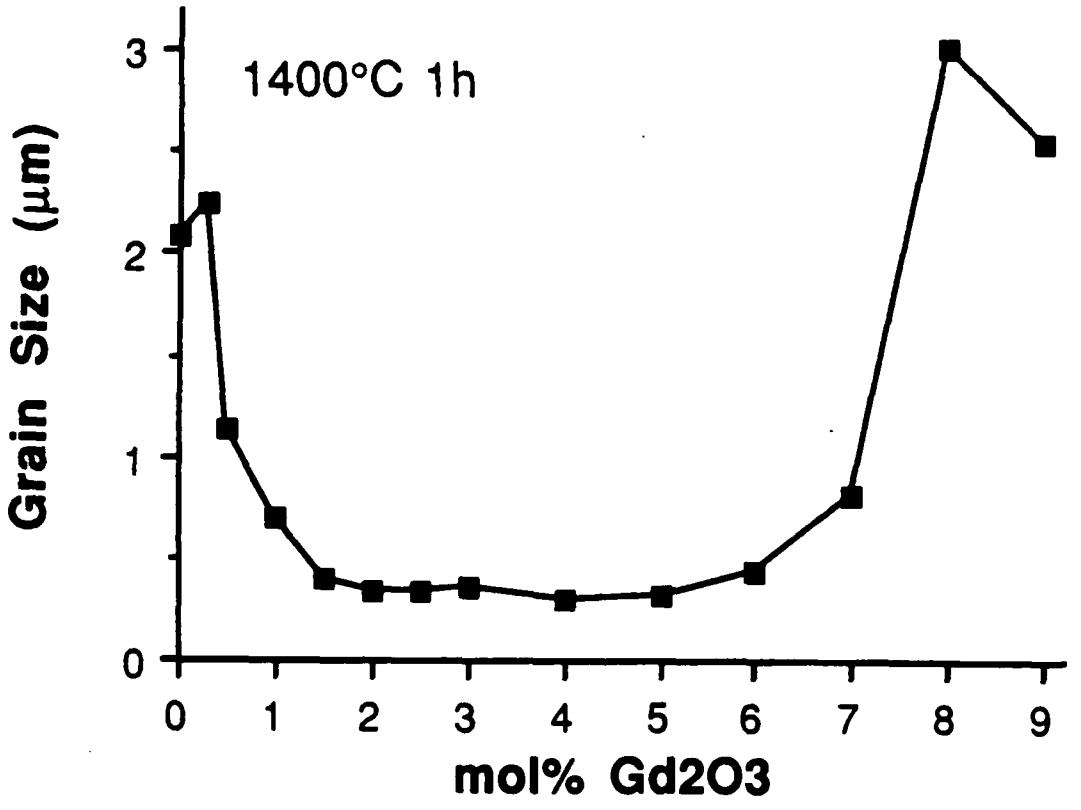

Figure 11. Average grain size of ZrO_2 with increasing Gd_2O_3 content heat treated at 1400°C for 1h.

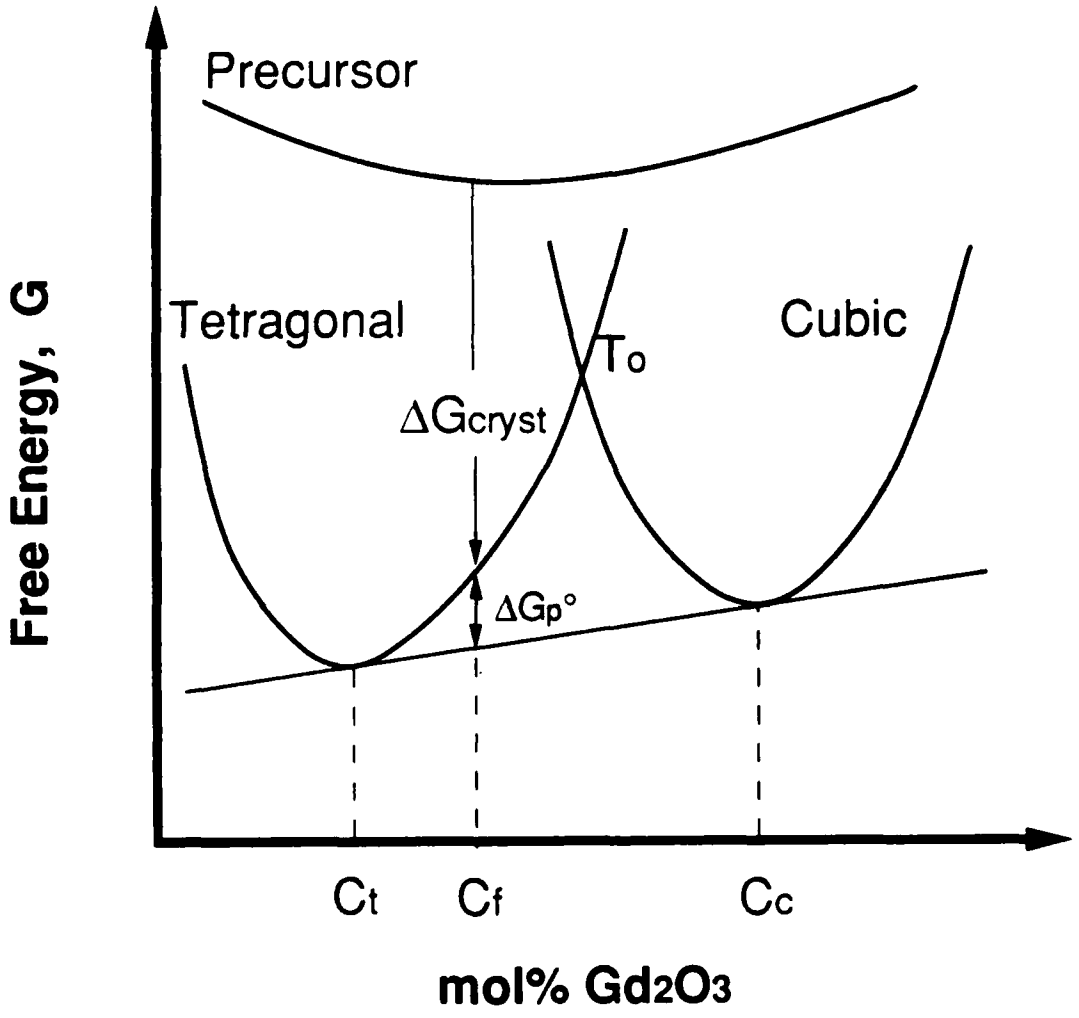

Figure 12. Schematic of free energy vs. composition for the tetragonal, cubic and disordered (glassy) phases at the temperature where the disordered phase, with composition C_f, crystallizes during precursor pyrolysis. C_t and C_c are the equilibrium compositions of the tetragonal and cubic structures, respectively, and T_o is the composition where the free energy of both tetragonal and cubic structures are identical.